AD

AD 729335

REPORT NO. RD-TR-71-12

TRANSONIC FLOW FIELDS AROUND VARIOUS BODIES OF REVOLUTION INCLUDING PRELIMINARY STUDIES ON VISCOUS EFFECTS WITH AND WITHOUT PLUME

SUMMARY REPORT

by

Jain-Ming Wu, Kinya Aoyama, and Trevor H. Moulden
University of Tennessee Space Institute
Tullahoma, Tennessee

May 1971

Approved for public release; distribution unlimited.

U.S. ARMY MISSILE COMMAND
Redstone Arsenal, Alabama

NATIONAL TECHNICAL
INFORMATION SERVICE

D D C
RECEIVED
SEP 15 1971
B

FORM AMSMI-1021, 1 DEC 65 PREVIOUS EDITION IS OBSOLETE

62

DISPOSITION INSTRUCTIONS

Destroy this report when it is no longer needed. Do not return it to the originator.

DISCLAIMER

The findings in this report are not to be construed as an official Department of the Army position unless so designated by other authorized documents.

ACC:
CFSTI
DDC
UNANNOUNCED
JUSTIFICATION
BY
DISTRIBUTION/AVAILABILITY CODES
DIST. AVAIL. and/or SPECIAL
A

TRADE NAMES

Use of trade names or manufacturers in this document does not constitute an official indorsement or approval of the use of such commercial hardware or software.

Security Classification

DOCUMENT CONTROL DATA - R & D

(Security classification of title, body of abstract and indexing annotation must be entered when the overall report is classified)

1. ORIGINATING ACTIVITY (Corporate author) Aeroballistics Directorate Directorate for Research, Development, Engineering and Missile Systems Laboratory U.S. Army Missile Command Redstone Arsenal, Alabama 35809	2a. REPORT SECURITY CLASSIFICATION UNCLASSIFIED 2b. GROUP N/A

3. REPORT TITLE

TRANSONIC FLOW FIELDS AROUND VARIOUS BODIES OF REVOLUTION INCLUDING PRELIMINARY STUDIES ON VISCOUS EFFECTS WITH AND WITHOUT PLUME

4. DESCRIPTIVE NOTES *(Type of report and inclusive dates)*

Technical Note

5. AUTHOR(S) *(First name, middle initial, last name)*

Jain-Ming Wu, Kinya Aoyama, and Trevor H. Moulden

6. REPORT DATE 27 May 1971	7a. TOTAL NO. OF PAGES 69	7b. NO. OF REFS 36
8a. CONTRACT OR GRANT NO. DAAH01-69-C-1357 b. PROJECT NO. (DA) 1M2326XXA206 AMC Management Structure Code c. No. 522C.11.14800 d.	9a. ORIGINATOR'S REPORT NUMBER(S) RD-TR-71-12 9b. OTHER REPORT NO(S) *(Any other numbers that may be assigned this report)*	

10. DISTRIBUTION STATEMENT

Approved for public release; distribution unlimited.

11. SUPPLEMENTARY NOTES None	12. SPONSORING MILITARY ACTIVITY Same as No. 1

13. ABSTRACT

This report outlines the solution to the lifting slender body in transonic flow. Remarks are also made concerning the transonic flow past cone-cylindrical configurations. Preliminary calculations concerning viscous effects, and particularly plume induced separation, are included.

DD FORM 1 NOV 65 1473 REPLACES DD FORM 1473, 1 JAN 64, WHICH IS OBSOLETE FOR ARMY USE.

UNCLASSIFIED
Security Classification

14. KEY WORDS	LINK A ROLE	LINK A WT	LINK B ROLE	LINK B WT	LINK C ROLE	LINK C WT
Inviscid flow studies						
Viscous flow studies						
Cone-cylindrical body						
Cone-cylindrical configuration						
Boundary layer solution						
Exhaust jet plume						

27 May 1971 Report No. RD-TR-71-12

TRANSONIC FLOW FIELDS AROUND VARIOUS BODIES OF REVOLUTION INCLUDING PRELIMINARY STUDIES ON VISCOUS EFFECTS WITH AND WITHOUT PLUME

SUMMARY REPORT

by

Jain-Ming Wu, Kinya Aoyama, and Trevor H. Moulden
University of Tennessee Space Institute
Tullahoma, Tennessee

DA Project No. 1M2326XXA206
AMC Management Structure Code No. 522C.11.14800
Supported by Contract No. DAAH01-69-C-1357

Approved for public release; distribution unlimited.

Aeroballistics Directorate
Directorate for Research, Development, Engineering
and Missile Systems Laboratory
U.S. Army Missile Command
Redstone Arsenal, Alabama 35809

ABSTRACT

This report outlines the solution to the lifting slender body in transonic flow. Remarks are also made concerning the transonic flow past cone-cylindrical configurations. Preliminary calculations concerning viscous effects, and particularly plume induced separation, are included.

FOREWORD

This report describes the results to date of an analysis conducted by the University of Tennessee Space Institute under U.S. Army Contract No. DAAH01-69-C-1357. The contract was initiated under DA Project No. 1M2326XXA206 and AMC Management Structure Code No. 522C.11.14800. The technical effort was performed between March 1970 and April 1971 under the direction of the Aerodynamics Group, Aeroballistics Directorate, U.S. Army Missile Command, Redstone Arsenal, Alabama. The Army technical representative was Mr. D. J. Spring.

CONTENTS

		Page
SECTION I.	INTRODUCTION	1
SECTION II.	INVISCID FLOW FIELD AROUND VARIOUS BODIES OF REVOLUTION	2
	1. Flow Field Around Ogive-Cylindrical Bodies at Small Angle of Attack	2
	2. Flow Field Along Nose Cones	15
	3. Flow Field Along Cone-Cylindrical Bodies	21
SECTION III.	CONCERNING VISCOUS EFFECTS	34
	1. Studies on Viscous/Inviscid Interactions	34
	2. Comments on Plume Induced Separation	37
SECTION IV.	CONCLUSIONS AND RECOMMENDATIONS	51
REFERENCES		53

ILLUSTRATIONS

Figure		Page
1	Nomenclature of Tangent Ogive Body	3
2	Variation of Side Surface Pressure with Angle of Attack at $M_\infty = 0.975$	9
3	Mach Number Contours on Leeward and Windward Planes for 5-Degree Angle of Attack at $M_\infty = 0.975$	10
4	Mach Number Contours on Leeward and Windward Planes for 5-Degree Angle of Attack at $M_\infty = 1.00$	11
5	Variation of Surface Pressure over Body Cross-Section at $M_\infty = 1.00$	12
6	Comparison of Present Theory with Experiments on Leeward Side for 2-Degree Angle of Attack at $M_\infty = 0.95$	13
7	Comparison of Present Theory with Experiments on Windward Side for 2-Degree Angle of Attack at $M_\infty = 1.05$	14
8	Nomenclature of Cone-Cylinder	16
9	Comparison of Various Methods with Data for 7-Degree Cone at Sonic Speed	22

Figure		Page
10	Comparison of Present Method with Local Linearization Method and Data at Sonic Speed.	23
11	Comparison of Present Method with Data for 10-Degree Cone at $M_\infty = 0.9$.	24
12	Comparison of Present Method with Data for 15-Degree Cone at $M_\infty = 1.10$	25
13	Calculated Flow Over Cone at 5-Degree Incidence and $M_\infty = 1.0$.	26
14	Surface Pressure Distribution on 10-Degree Cone at $M_\infty = 1.0$ (at $x/\ell = 0.75$ Station)	27
15	Comparison of Theory with Data for a Cone at Various Angles of Attack.	28
16	Flow Over a Blunted 15-Degree Cone at $M_\infty = 0.9$.	29
17	Calculated Flow for Cone-Cylindrical Body at $M_\infty = 0.96$.	31
18	Calculated Flow for Cone-Cylindrical Body at $M_\infty = 1.00$.	32
19	Calculated Flow for Cone-Cylindrical Body at $M_\infty = 1.04$.	33
20	Calculated Boundary Layer for $M_\infty = 0.975$ and Re = 1.2×10^6/ft.	38
21	Calculated Correction to Surface Pressure Distribution.	38
22	Sensitivity of Boat Tail Boundary Layer to Initial Conditions.	41
23	Comparison of Separation Pressures in Two-Dimensional Axisymmetric Flow (Turbulent Boundary Layers)	42
24	The Confluence Region	45
25	Four-Calibre Tangent Ogive Body Used in Plume Study Calculations.	47
26	Some Results at $M_\infty = 2.0$.	48
27	Increase of Flow Separation with Jet Pressure Ratio at $M_\infty = 1.1$	49
28	Interaction of Plume with Fore-Body Flow at $M_\infty = 1.1$.	50

Section I. INTRODUCTION

The progress made since publication of our last summary report [1] is summarized and reported herein. Considerable knowledge was obtained in the inviscid flow field, which is necessary before one can study in detail the viscous flow field and interaction on various bodies of revolution including small angles of attack. The studies on viscous effects are preliminary ones; however, some interesting results as well as the direction of future investigations are pointed out. Since this is a summary report, most details were omitted; however, a series of publications which present the calculation procedures as well as detail discussions are referenced.

The major ideas and typical results on the inviscid and the viscous flow studies are presented in Sections II and III, respectively. The analysis on inviscid transonic flow field around an ogive-cylindrical body at zero angle of attack [2] has been extended to include the effect of cross-flow caused by small angles of attack. The results are very encouraging and check reasonable well with experiments including recent investigations by AMICOM. The flow over a conical nose shape has been solved using the integral approach for the entire transonic flow regime. It will be shown that this is a higher order approximation method. The analysis can take into account the cone at small angles of attack with good agreement with the available data. This study has been extended to calculate the flow field along a cone-cylindrical body at zero angle of attack where the method used for the cylindrical body portion has been reported in previous publications [1, 3].

The effect of viscous and inviscid flow interaction is studied by considering the boundary layer build up, including transition and through a normal shock wave, and its results upon the inviscid flow field. (The interaction between the potential solution and the boundary layer solution is studied through the iteration process.) Remarks concerning the usually accepted "equivalent body" concept are noteworthy, especially, if separation is involved. A preliminary study on the separation caused by the exhaust jet plume indicates that the transonic separation could be very different from that of the lower supersonic case. Moreover, if the separated region is small, the usually accepted "equilibrated" free shear layer analysis is not applicable.

A very basic study program on the transonic separation problem has been initiated. Studies involving problems in improving the inviscid flow solutions are continuously in progress.

Section II. INVISCID FLOW FIELD AROUND VARIOUS BODIES OF REVOLUTION

The nonlinear correction theory with stretching procedure has been extended to a lifting ogive-cylindrical body. The solutions were obtained over the entire transonic flow regime. The major ideas and some results are presented in Paragraph 1. The integral equation approach to the flow field along a conical nose is discussed in Paragraph 2. The complete solution over a nonlifting cone-cylindrical body is discussed in Paragraph 3.

1. Flow Field Around Ogive-Cylindrical Bodies at Small Angle of Attack

a. Basic Consideration

It has been shown [1, 2] that Hosokawa's nonlinear correction theory [4, 5] with a stretching procedure [2] can be applied to a cylindrical body with an ogive nose at zero angle of attack. The surface pressure distributions as well as shock wave locations over various body configurations have been shown to agree fairly well with experiments. Encouraged by these good agreements, an extension to include the body at small angle of attack has been attempted. The following discussion only presents the major idea and the detailed approach is in preparation as a separate publication*.

The appropriate inviscid transonic flow small perturbation equation can be written

$$\left(1 - M_\infty^2\right)\Phi_{xx} + \frac{1}{r}\frac{\partial}{\partial r}\left(r\Phi_r\right) + \frac{1}{r^2}\frac{\partial^2\Phi}{\partial\theta^2} = (\gamma + 1)\, M_\infty^2\, \Phi_x\Phi_{xx} \qquad (1)$$

in which the velocity potential, Φ, is normalized with respect to the free-stream velocity U_∞. The coordinates and the geometry are illustrated in Figure 1. A solution must satisfy the boundary conditions of tangential flow at the body surface with the perturbation velocities vanishing at infinity.

The tangential boundary condition can be approximated for a slender body by

*Wu, J. M. and Aoyama, K., Transonic Field Around Ogive-Cylinder at Small Angle of Attack, U.S. Army Missile Command, Redstone Arsenal, Alabama, Technical Report (to be published soon), 1971.

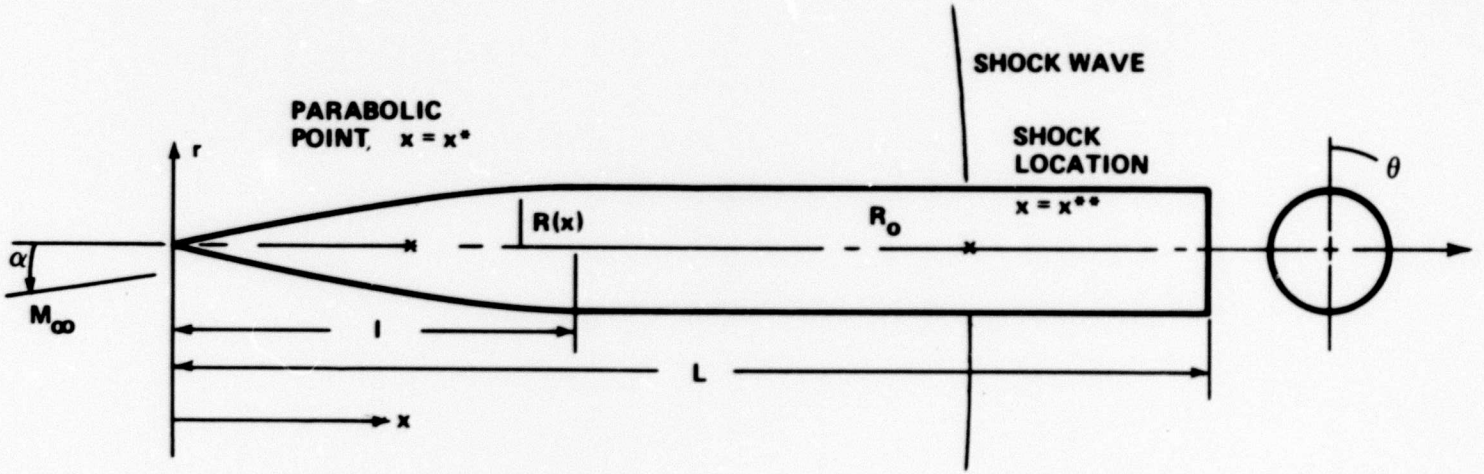

Figure 1. Nomenclature of Tangent Ogive Body

$$\left[\Phi_r + \text{Sin}\ \alpha\ \text{Cos}\ \theta\right]_{\text{on body}} \simeq \frac{dR}{dx} \tag{2}$$

where α and R are the angle of attack given in radians and the normalized body radius with respect to the total body length L, respectively.

In Hosokawa's nonlinear correction theory [5], the nonlinear solution Φ of Equation (1) is assumed to be formed by the linearized solution ϕ of Oswatitsch and Keune [6] type and a correction function g. ϕ is a solution of the equation which reads

$$\left(1 - M_\infty^2\right)\phi_{xx} + \frac{1}{r}\frac{\partial}{\partial r}\left(r\phi_r\right) + \frac{1}{r^2}\frac{\partial^2\phi}{\partial\theta^2} = K\phi_x \tag{3}$$

where the contribution from the azimuth direction is included because of the cross flow induced by the small angle of attack. K is an acceleration like term and has been assumed to be a constant. This assumption leads to the so-called "parabolic" method known to the technical community. Hosokawa assumed that

$$\Phi = \phi + g \tag{4}$$

where g is the correction function. A further study on this g function is underway and will be in a separate technical report*.

By Equations (1), (3), and (4), and by order of magnitude arguments [5], it has been found that the g function has to satisfy the following equation:

$$\frac{\partial}{\partial x}\left\{\left[\left(M_\infty^2 - 1\right) + (1 - \gamma)\ M_\infty^2\ \phi_x\right] g_x + \frac{1+\gamma}{2}\ M_\infty^2\ g_x^2\right\}$$
$$= -\left[(1 + \gamma)\ M_\infty^2\ \phi_{xx} - K\right]\phi_x. \tag{5}$$

The correction function g may be understood to be a function of x with r and θ as parameters, i.e., $g(x;r,\theta)$. Integration of Equation (5) gives

*Wu, J. M., Some Remarks on Transonic Flow Nonlinear Correction Theory (in preparation).

$$g_x\ (x;r,g) \quad = \quad - \left[\phi_x - \frac{1-M_\infty^2}{(1+\gamma)M_\infty^2} \right] \pm \sqrt{Y\ (x)} \tag{6}$$

where

$$Y(x) \quad = \left[\phi_x - \frac{1-M_\infty^2}{(1+\gamma)M_\infty^2} \right]^2 - \ 2 \int_{x^*}^{x} \left[\phi_{xx} - \frac{K}{(\gamma+1)M_\infty^2} \right] \phi_x \, d_x$$

in which x^* is the unknown parabolic point where the coefficient of ϕ_{xx} in the nonlinear transonic equation vanishes.

The double sign of Equation (6) is determined according to the first term on the right side of Equation (6) [2, 5], i.e.,

$$\phi_x \ - \ \frac{1-M_\infty^2}{(\gamma+1)M_\infty^2} \ \gtrless \ 0 \ . \tag{7}$$

It is suggested that the parabolic point x^* is determined such that the x component of perturbation velocity determined from the linearized transonic equation, gives the nonlinear solution at that point, i.e.,

$$\phi_x\ (x^*;r,\theta\ ) \ = \ \ \phi_x\ (x^*;r,\theta\ ) \ = \ \frac{1-M_\infty^2}{(\gamma+1)M_\infty^2} \ . \tag{8}$$

This satisfies the condition that the acceleration is continuous in the accelerated flow regime. From comparison of Equations (1) and (3) with Equation (8), one obtains,

$$\phi_{xx}\ \ (x^*;r,\theta) \ = \ \frac{K}{(1+\gamma)M_\infty^2} \ . \tag{9}$$

Therefore, Equations (8) and (9) are the two equations which determine the two unknowns, K and x^*. The nonlinear solution, can thus, be constructed according to Equation (4) with Equation (6) as follows:

$$\phi_x = \frac{1-M_\infty^2}{(\gamma+1)M_\infty^2} \ \pm \ \sqrt{Y(x)} \tag{10}$$

where

$$Y(x) = -2\,\phi_x(x^*)\left[\phi_x(x) - \phi_x(x^*)\right] + \frac{2K}{(\gamma+1)M_\infty^2}\left[\phi(x) - \phi(x^*)\right] .$$

The linear perturbation potential is assumed to be expressible as the sum of two parts because of the axial flow and the cross flow. This assumption is valid only if the angle of attack is small and no boundary layer separation is present in the flow field. This gives

$$\phi\,(x,r,\theta) = \phi_a\,(x,r) + \phi_c\,(x,r,\theta) \tag{11}$$

where ϕ_a and ϕ_c denote the axial and cross flow, respectively.

By the linearized small perturbation Equation (3), the governing equations for ϕ_a and ϕ_c read

$$\left(1 - M_\infty^2\right)\phi_{a_{xx}} + \frac{1}{r}\frac{\partial}{\partial r}\left(r\,\phi_{a_r}\right) = K\,\phi_{a_x} \tag{12}$$

and

$$\left(1 - M_\infty^2\right)\phi_{c_{xx}} + \frac{1}{r}\frac{\partial}{\partial r}\left(r\,\phi_{c_r}\right) + \frac{1}{r^2}\frac{\partial^2\,\phi_c}{\partial\theta^2} = K\,\phi_{c_x} . \tag{13}$$

The solution for the axial flow ϕ_a has been discussed in detail by Wu and Aoyama [2]. The discussion on the solution for the cross flow ϕ_c is given by Liepmann and Roshko [7]. The simplified cross flow solution reads

$$\phi_c\,(x,r,\theta) = \cos\theta\,\frac{\partial\,\phi_a}{\partial r} = \sin\alpha\cos\theta\,\frac{R^2(x)}{r} . \tag{14}$$

The last expression is known as the Munk-Jones cross flow term.

The boundary condition, Equation (2), can be rewritten* for the linear solution as follows:

*For details, see Wu and Aoyama, loc. cit.

$$\phi_{a_r}\Big|_{body} = \frac{dR}{dx} \tag{15}$$

and

$$\left(\phi_{c_r} + \text{Cos}\ \theta\ \text{Sin}\ \alpha\right)\Big|_{body} = 0 \quad . \tag{16}$$

Now, if the angle of attack is small, it is reasonable to assume that the linear perturbation velocity may be expressed as

$$\phi\ (x,r,\theta) = \phi_o\ (x,r) + \triangle\ \phi\ (x,r,\theta) \tag{17}$$

where the subscript o denotes the basic solution at zero angle of attack, i.e., the axial flow solution. Thus, by comparison of Equations (11) and (17), one identifies $\triangle\ \phi$ with the Munk-Jones cross flow term. However, it should be noted that ϕ_o is not the same solution of the axisymmetric equations discussed in reference [2], because of the shift in the sonic point location and the change in the constant K.

By the conditions set out in Equations (8) and (9), one obtains

$$\phi_{o_x}\left(x_o^* + \Delta x^*,\ K_o + \triangle K\right) + \triangle\phi_x\left(x_o^* + \triangle x^*,\ K_o + \triangle K\right) = \left(1 - M_\infty^2\right) \ / \ (1+\gamma)M_\infty^2 \tag{18}$$

and

$$\phi_{o_{xx}}\left(x_o^* + \triangle x^*,\ K_o + \triangle K\right) + \triangle\ \phi_{xx}\left(x_o^* + \triangle x^*,\ K_o + \triangle K\right) = \frac{\left(K_o + \triangle K\right)}{(1+\gamma)M_\infty^2} \tag{19}$$

where x_o^* and K_o are the solutions based on the axisymmetric solution [2].

The nonlinear perturbation velocity Φ_x, finally reads

$$\Phi_x = \frac{1-M_\infty^2}{(\gamma+1)M_\infty^2} \pm \sqrt{Y_o + \triangle Y} \tag{20}$$

where Y_o is due to the axial flow and $\triangle Y$ is due to the small angle of attack. The expressions for Y_o and $\triangle Y$ are:

$$Y_o(x) = -2\frac{1-M_\infty^2}{(1+\gamma)M_\infty^2}\left[\phi_{o_x}(x) - \frac{1-M_\infty^2}{(1+\gamma)M_\infty^2}\right] + \frac{2K_o}{(1+\gamma)M_\infty^2}\left[\phi_o(x) - \phi_o\left(x_o^*, K_o\right)\right] \tag{21}$$

and

$$\triangle Y(x) = -2\frac{1-M_\infty^2}{(1+\gamma)M_\infty^2}\triangle\phi_x(x) + \frac{2\triangle K}{(1+\gamma)M_\infty^2}\phi_o(x) + \frac{2K_o}{(1+\gamma)M_\infty^2}\left[\triangle\phi(x) - \triangle K\phi_{o_x}\left(x_o^*, K_o\right) - \triangle x^*\phi_{o_x}\left(x_o^*, K_o\right)\right] \tag{22}$$

therefore, the correction of Y(x) due to the angle of attack can be performed.

b. Discussions of Solutions and Comparisons with Data

Without going into details (which will be published as a separate report*), some typical solutions are presented in Figures 2 through 7.

The pressure distribution along the $\theta = 90$ degree surface changes with angle of attack as illustrated in Figure 2. An increase in angle of attack increases the shock wave strength as expected. In the

*Wu and Aoyama, loc. cit.

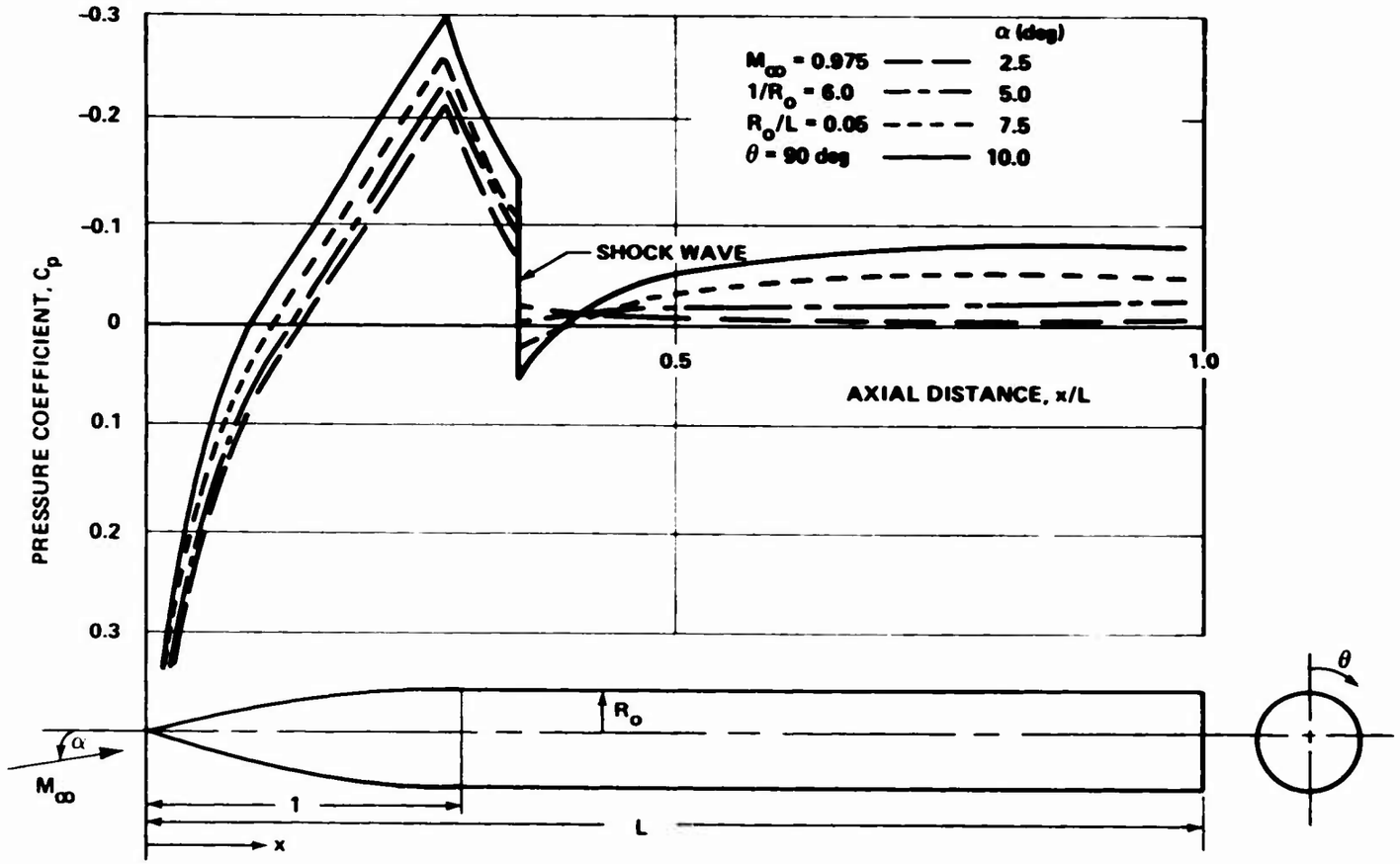

Figure 2. Variation of Side Surface Pressure with Angle of Attack at M_∞ = 0.975

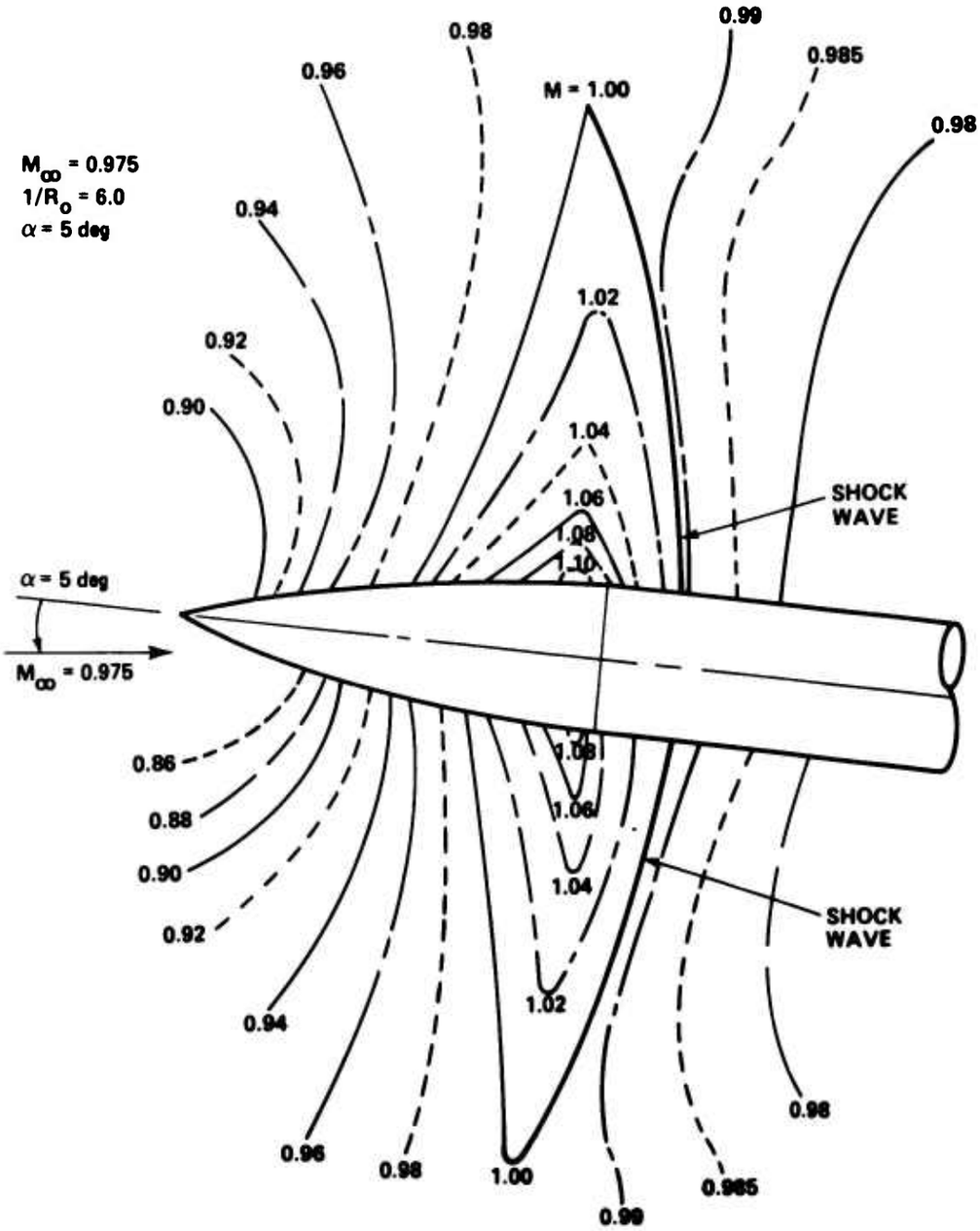

Figure 3. Mach Number Contours on Leeward and Windward Planes for 5-Degree Angle of Attack at M_∞ = 0.975

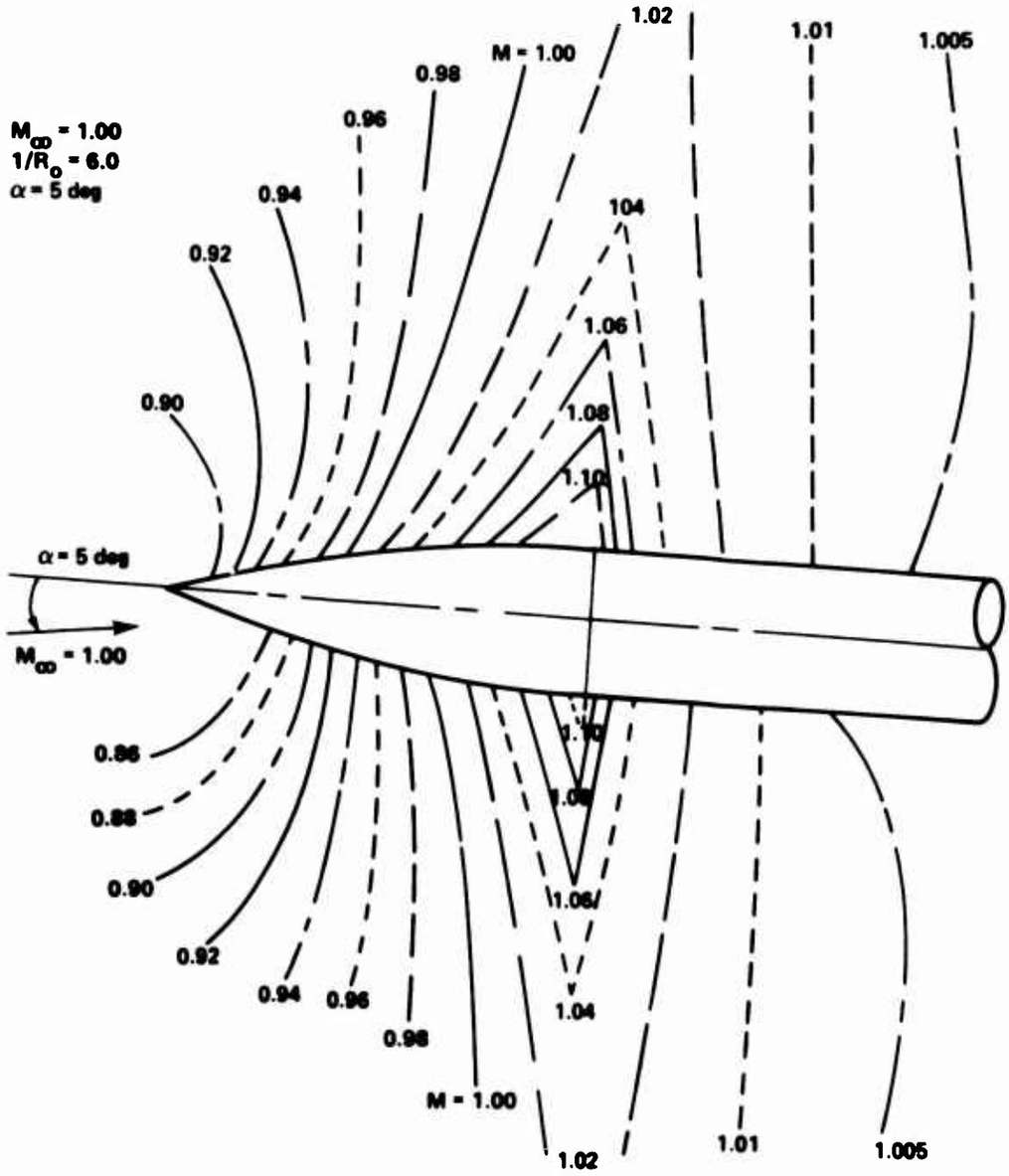

Figure 4. Mach Number Contours on Leeward and Windward Planes for 5-Degree Angle of Attack at M_∞ = 1.00

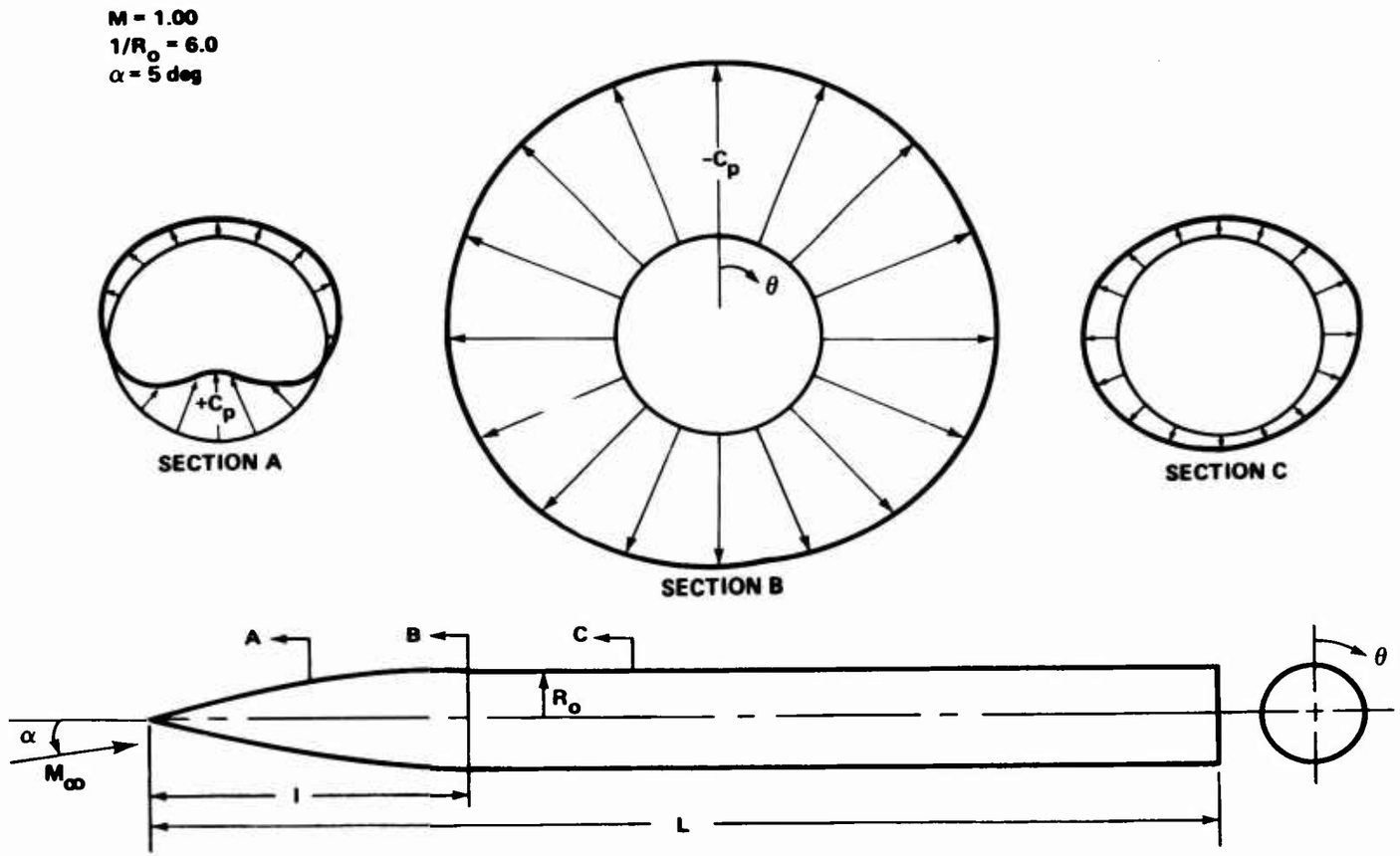

Figure 5. Variation of Surface Pressure Over Body Cross-Section at $M_\infty = 1.00$

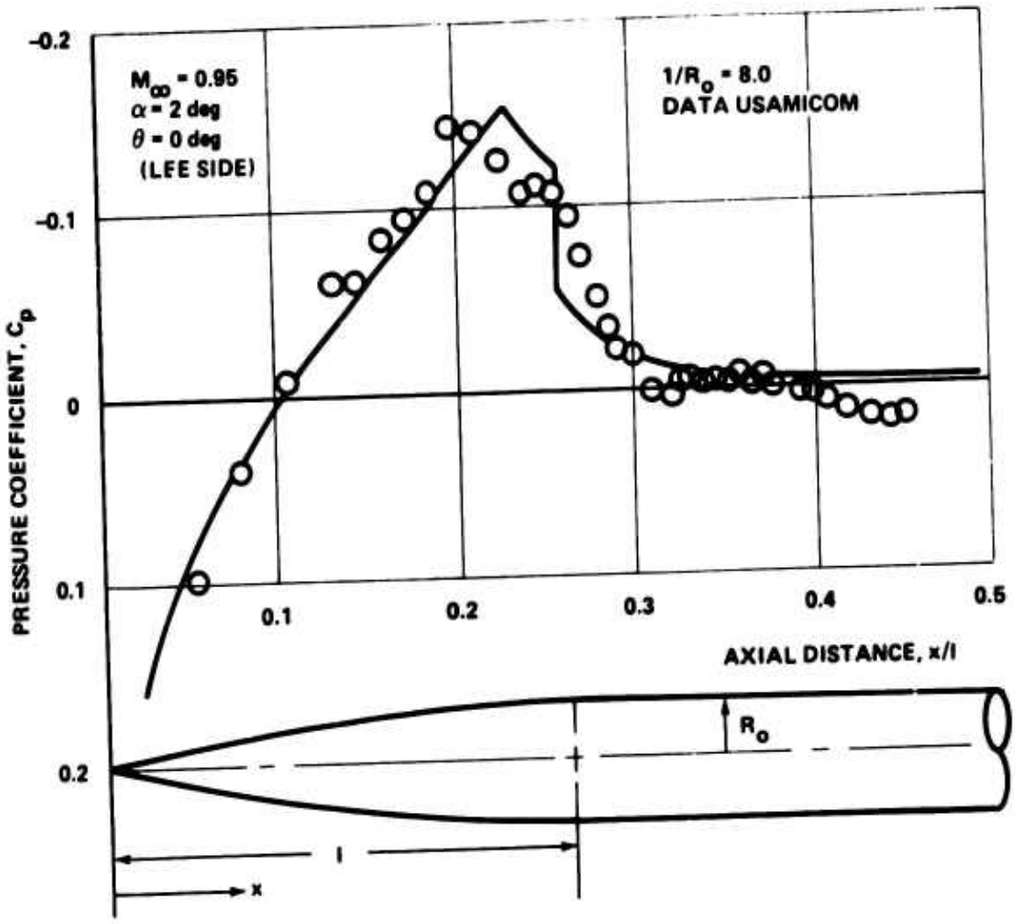

Figure 6. Comparison of Present Theory with Experiments Leeward Side for 2-Degree Angle of Attack at M_∞ = 0.95

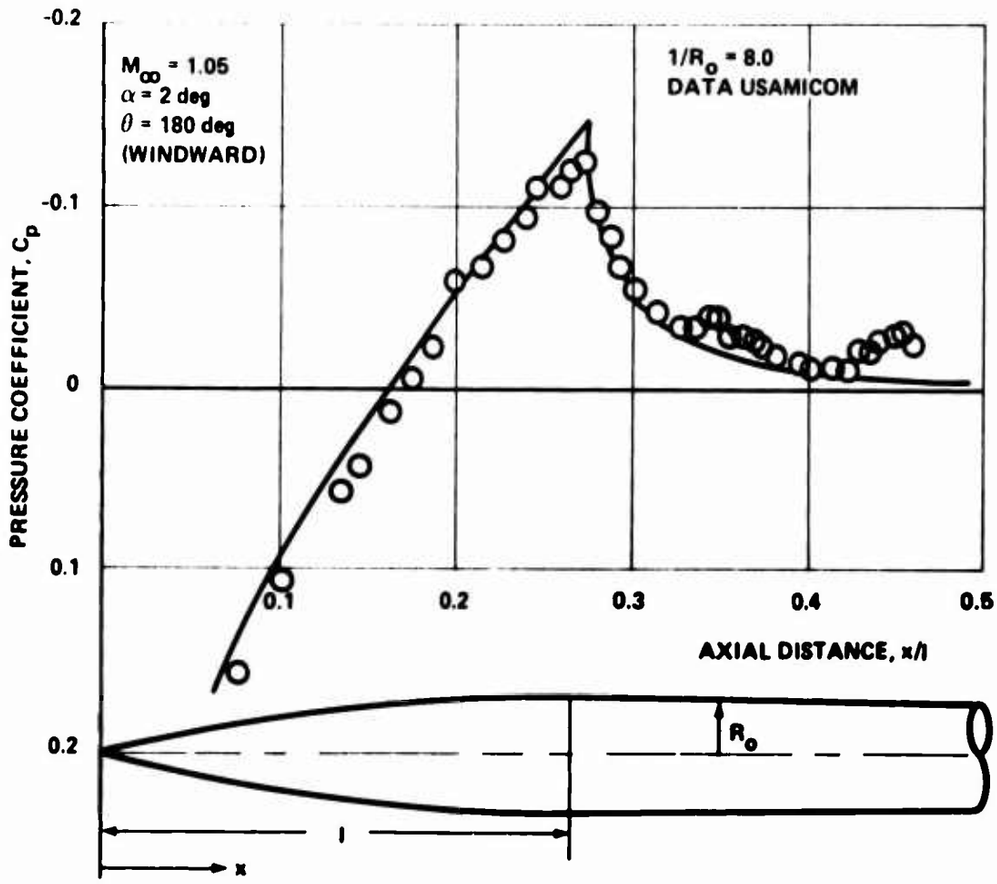

Figure 7. Comparison of Present Theory with Experiments on Windward Side for 2-Degree Angle of Attack at M_∞ = 1.05

axisymmetric flow case [2], the pressure coefficient along the cylindrical body vanishes. However, this is not so in the angle of attack case because of the cross flow.

The entire flow field, disturbed by the presence of a body, is illustrated in Figures 3 and 4 for a subsonic and a sonic free stream case, respectively, for the plane including the leeward and the windward variations. The flow pattern on the leeward side changes more gradually compared with the windward side. It can be seen in Figure 3 that the movement of the sonic point is more sensitive to the movement of the shock location at angle of attack.

Figure 5 presents an indication of the circumferential pressure distributions at various stations. The suction reaches a maximum near the shoulder. The major lift component comes from the front portion of the body. On the cylindrical portion of the body, the cross flow contribution is more significant.

A comparison was made with recent AMICOM data for various angles of attack over the entire transonic flow region and the agreement is very good. Two typical examples of windward and leeward pressure distributions compared with the theory are presented in Figures 6 and 7, respectively. More comparisons will be included in future publications. The inclusion of the viscous effect will be discussed in Section III.

2. Flow Field Along Nose Cones

a. Basic Consideration

The analysis of the inviscid flow around a conical body at various transonic speeds has been performed with much success. This is very encouraging, in view of the fact that the existing available techniques are restricted to a free stream of Mach number 1 (or a very minor perturbation from 1). Moreover, the present method can also take care of the small angle of attack case.

The appropriate small disturbance transonic flow equation is Equation (1), given in Paragraph 1. For the present case, all the lengths are normalized with respect to the axial length of the cone (Figure 8). Now, in case of the transonic flow past a cone, it is a well known fact that the sonic velocity is fixed at the shoulder, and the flow is subsonic over the entire conical forebody, as long as the angle of attack is small and the shock wave is not attached to the body.

Rewriting the nonlinear transonic equation, Equation (1), as

$$\left[\left(1-M_\infty^2\right) - (1+\gamma)M_\infty^2 \frac{\partial \phi}{\partial x} \right] \frac{\partial^2 \phi}{\partial x^2} + \frac{1}{r}\frac{\partial}{\partial r}\left(r \frac{\partial \phi}{\partial r}\right) + \frac{1}{r^2}\frac{\partial^2 \phi}{\partial \theta^2} = 0 \qquad (1')$$

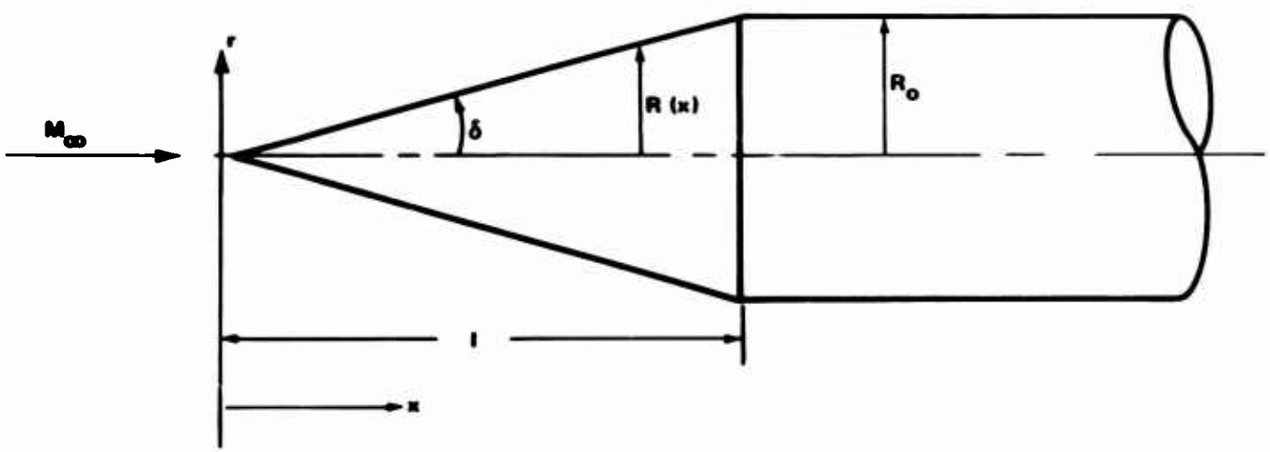

Figure 8. Nomenclature of Cone Cylinder

then, the above observation for subsonic flow over the entire forebody suggests that the coefficient of Φ_{xx} has to be positive and nonzero. This inspired the following linearization technique:

$$\left(1-M_\infty^2\right) - (1+\gamma)M_\infty^2 \, \Phi_x = f^2(x) \tag{23}$$

where f(x) is an unknown function which will be determined later. This approach is somewhat similar to that devised by Cole and Royce [8] in which $\partial\phi/\partial x$ is approximated but $\partial^2\phi/\partial x^2$ is not.

Now, by introducing a new independent variable ξ such that

$$f\left[x(\xi)\right] = \frac{dx}{d\xi} \tag{24}$$

the original equation, Equation (1') is reduced to

$$\frac{\partial^2\phi}{\partial\xi^2} + \frac{1}{r}\frac{\partial}{\partial r}\left(r\frac{\partial\phi}{\partial r}\right) + \frac{1}{r^2}\frac{\partial^2\phi}{\partial\theta^2} = 0 \tag{25}$$

which is a Laplace equation, and ϕ is the linearized velocity potential normalized with respect to the free stream velocity.

As approximated in Paragraph 1, assume that the perturbation velocity potential ϕ is composed of the axial flow contribution ϕ_a and the cross flow term ϕ_c is due to the small angle of attack. This gives

$$\phi(\xi,r,\theta) = \phi_a(\xi,r) + \phi_c(\xi,r,\theta) \quad . \tag{26}$$

The appropriate boundary conditions for ϕ_a and ϕ_c are

$$\phi_c(\xi,r,\theta) = \sin\alpha\cos\theta \; R^2(\xi)/r \tag{27}$$

and

$$\left.\frac{\partial\phi_a(\xi,r)}{\partial r}\right|_{\text{body surface}} = 0 \tag{28}$$

where δ is the half-angle of the cone measured in radians.

The fundamental solution to Equation (25) for ϕ_a is

$$\phi_a(\xi, r) = -\frac{1}{4\pi} \int_0^{\xi^*} \frac{F(t)}{\sqrt{(\xi - t)^2 + r^2}} \, dt \qquad (29)$$

where ξ^* is the sonic velocity point in the transformed plane corresponding to the shoulder location, and F(t) is the source distribution along the body axis determined by the boundary condition of the problem, respectively.

Without going into details (the details will be published as a separate report*), it is found that

$$\frac{\partial \phi_a}{\partial r} = \frac{F(\xi)}{2\pi r} \qquad (30)$$

where the source distribution $F(\xi)$ satisfies

$$F(\xi) = 2\pi \cdot R(\xi) = 2\pi \delta^2 X(\xi) \quad . \qquad (31)$$

The relation between X and ξ is, from Equation (24),

$$X(\xi) = \int_0^{\xi} f(t) \, dt \quad . \qquad (32)$$

Therefore,

$$F(\xi) = 2\pi \delta^2 \int_0^{\xi} f(t) \, dt \qquad (33)$$

and, with Equations (29) and (26), one obtains the velocity potential as,

*Wu, J. M., and Aoyama, K., On Transonic Flow Past a Cone-Cylinder Body with and Without Angle of Attack, U.S. Army Missile Command Technical Report, Redstone Arsenal (to be published soon), 1971.

$$\phi(\xi,r) = -\frac{\delta^2}{2}\int_0^{\xi^*} \frac{\int_0^t f(s)ds}{\sqrt{(\xi-t)^2 + r^2}}\, dt$$

$$+ \sin\alpha \cos\alpha \frac{1}{r}\, \delta^2 \left[\int_0^{\xi} f(t)\, dt\right]^2 . \tag{34}$$

To obtain the expression for $f(\xi)$, following Equation (34), one obtains

$$\frac{\partial\phi}{\partial\xi} = \frac{\delta^2}{2}\frac{1}{\sqrt{(\xi-\xi^*)^2 + r^2}} - \frac{\delta^2}{2}\left[\int_0^{\xi^*} \frac{f(t)}{\sqrt{(\xi-t)^2 + r^2}}\, dt\right]$$

$$+ 2\frac{\delta^2}{r} \sin\alpha \cos\alpha\, f(\xi)\left[\int_0^{\xi} f(t)\, dt\right] . \tag{35}$$

However,

$$\frac{\partial\phi}{\partial\xi} = \frac{\partial x}{\partial\xi}\frac{\partial\phi}{\partial x} = f(\xi)\left[\frac{1-M_\infty^2 - f^2(\xi)}{(\gamma+1)M_\infty^2}\right] \tag{36}$$

where the relation between $\partial\phi/\partial x$ and $f(\xi)$ in Equation (23) was employed. Then, Equations (35) and (36) are reduced to the following integral equation along the body surface,

$$\left[f(\xi)\right]^3 = \left[\left(1-M_\infty^2\right) - 2\delta(1+\gamma) M_\infty^2 \sin\alpha \cos\alpha\right] f(\xi)$$

$$+ \frac{1}{2}\delta^2 (1+\gamma) M_\infty^2 \left[\int_0^{\xi^*} \frac{f(t)\, dt}{\sqrt{(\xi-t)^2 + R^2(\xi)}} - \frac{1}{\sqrt{(\xi-\xi^*)^2 + R^2(\xi)}}\right] . \tag{37}$$

The function $f(\xi)$, which behaves as the square root of the perturbation velocity, must satisfy the boundary conditions at the apex and at the shoulder. At the apex where $x = 0$, the stagnation condition requires

$$U_\infty + U_\infty \phi_x = 0 \tag{38}$$

or

$$\Phi_x = -1 \quad . \tag{38'}$$

From Equation (23) and by Equation (38'), the solution should asymptotically behave as

$$f(o) = \left[\left(1-M_\infty^2\right) + (1+\gamma)M_\infty^2\right]^{1/2} \quad . \tag{39}$$

At the sonic point where $\xi = \xi^*$, one expects

$$f(\xi^*) = 0 \quad . \tag{40}$$

By employing Equation (32), the sonic velocity location is at the shoulder and is determined by the condition

$$\int_0^{\xi^*} f(t)\, dt = 1 \quad . \tag{41}$$

With these boundary conditions, the nonlinear integral equation, Equation (37), is solved for f (ξ)*. The velocity potential is then obtained by

$$\Phi_x(\xi) = \frac{\left(1-M_\infty^2\right) - \left[f(\xi)\right]^2}{(\gamma+1)M_\infty^2} \quad . \tag{42}$$

Then, x (ξ) is related to f (ξ) by the condition of Equation (32). The pressure coefficient on the body surface is determined by

$$Cp = -2\,\Phi_x - \xi^2 + (1-4\,\mathrm{Sin}^2\,\gamma)\,\mathrm{Sin}^2\,\alpha \quad . \tag{43}$$

*For the details of solving Equation (37), see Wu and Aoyama, loc. cit.

b. Discussions of Solutions and Comparisons with Data

The limited available theories, which were developed by quite different approaches for sonic flow over a cone-cylindrical body, are compared to the present theory. The available theories are the local linerization method of Sprieter and Alksne [9], Yashihara's numerical approximation [10], and Leiter and Oswatitsch's time dependent characteristic method [11]. These are compared to the original data of Page [12] and the present theory in Figure 9. The present result and Leiter and Oswatitsch's fall very close to each other and agree very well with the data.

It may be noted that the present theory predicts reasonable values along the center portion of the cone. The theory predicts a somewhat poorer solution near the shoulder because of the approximation used in solving the integral equation for $f(\xi)$ (discussed in detail in a report to be published). The poor agreement near the apex point is caused by violating the small disturbance assumption. Treating the apex and the shoulder as singular points and matching of the asymptotic solutions agree with the present result away from the singularity.

The applicability of the present method to flows other than the sonic flow are demonstrated in Figures 10, 11, and 12. The agreement of the data for the slightly subsonic flow of Figure 11 and slightly supersonic flow of Figure 12 is very encouraging.

Typical results for bodies at small angles of attack are shown in Figures 13 and 14. It can be seen that the pressure change with azimuth angle is rather significant on the windward side. In Figure 15, the variation of pressure distribution resulting from different angles of attack is shown. A comparison with data is also given in Figure 16 for a slightly blunted cone at a 6-degree angle of attack.

3. Flow Field Along Cone-Cylindrical Bodies

The analytical treatment of the flow downstream of the sharp shoulder of a cone-cylindrical body configuration has been studied and reported [3]. Therefore, by matching the cone-solution as described in Paragraph 2 to the developed local two-dimensional approximation method, it is possible to obtain the complete "on body" solution for a cone-cylindrical body at zero angle of attack. The restriction to zero angle of attack is because the work derived and reported in reference [3] was based upon the axisymmetric condition.

From the conical-nose portion of the analysis, the local Mach number at the shoulder has been taken as unity in transonic flow. A Prandtl-Meyer expansion around the corner is then assumed. The local two-dimensional approximation method permits transformation between the axisymmetric and the two-dimensional bodies. The final result for the

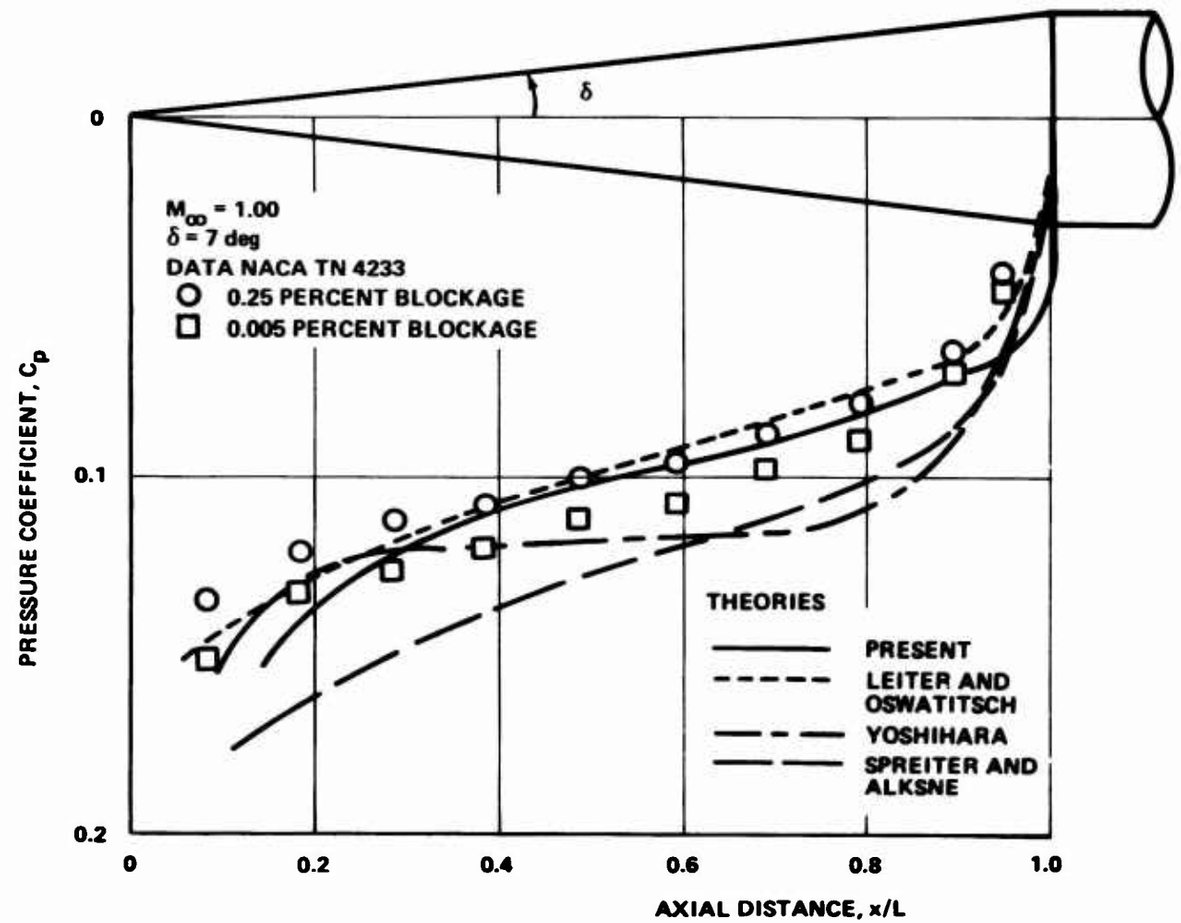

Figure 9. Comparison of Various Methods with Data for 7-Degree Cone at Sonic Speed

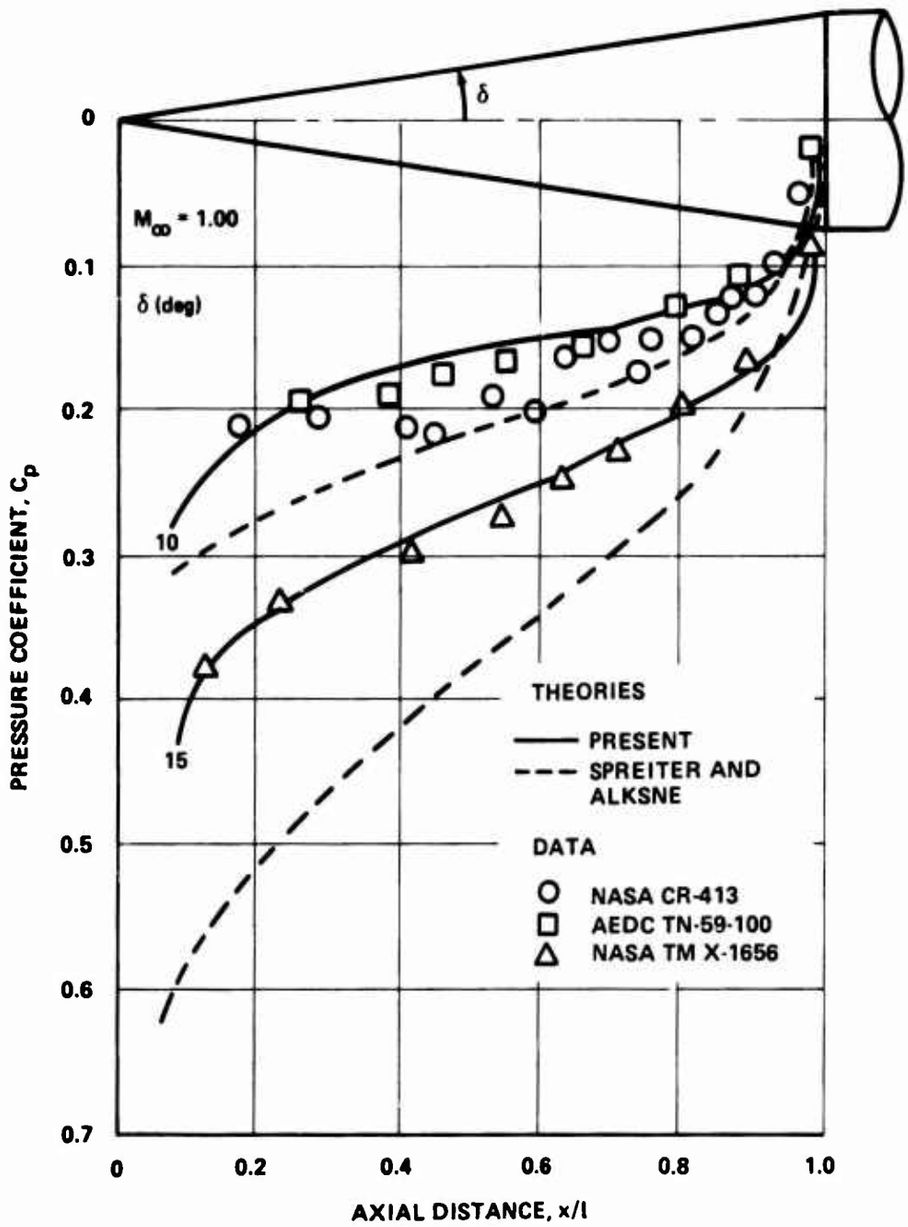

Figure 10. Comparison of Present Method with Local Linearization Method and Data at Sonic Speed

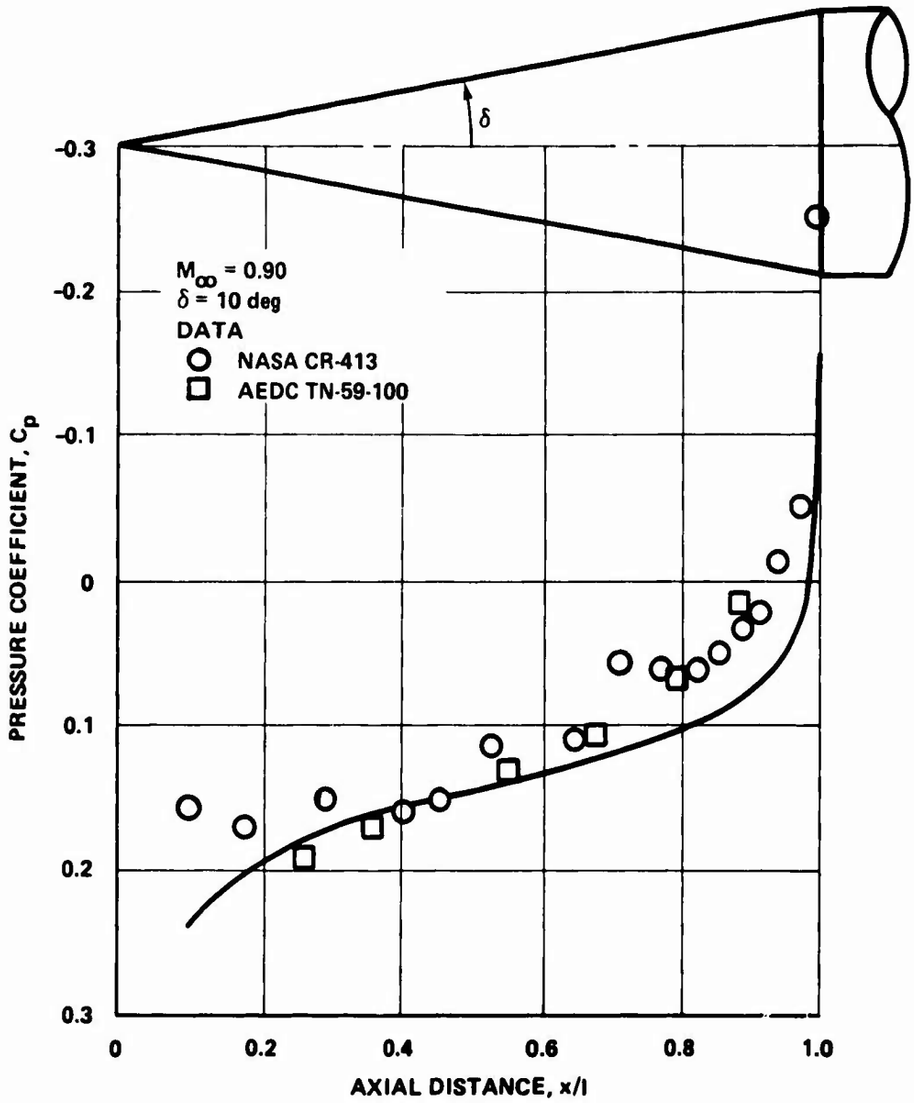

Figure 11. Comparison of Present Method with Data for 10-Degree Cone at M_∞ = 0.9

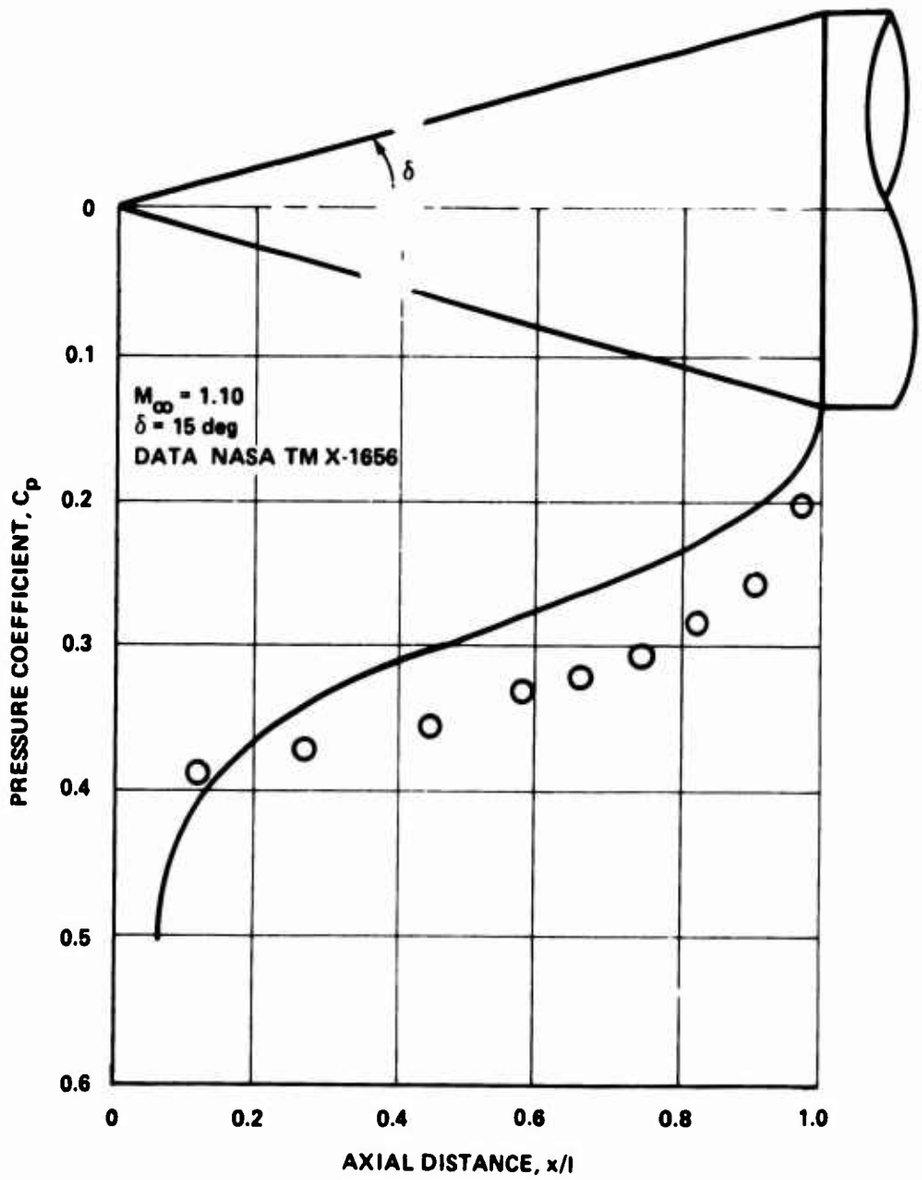

Figure 12. Comparison of Present Method with Data for 15-Degree Cone at $M_\infty = 1.10$

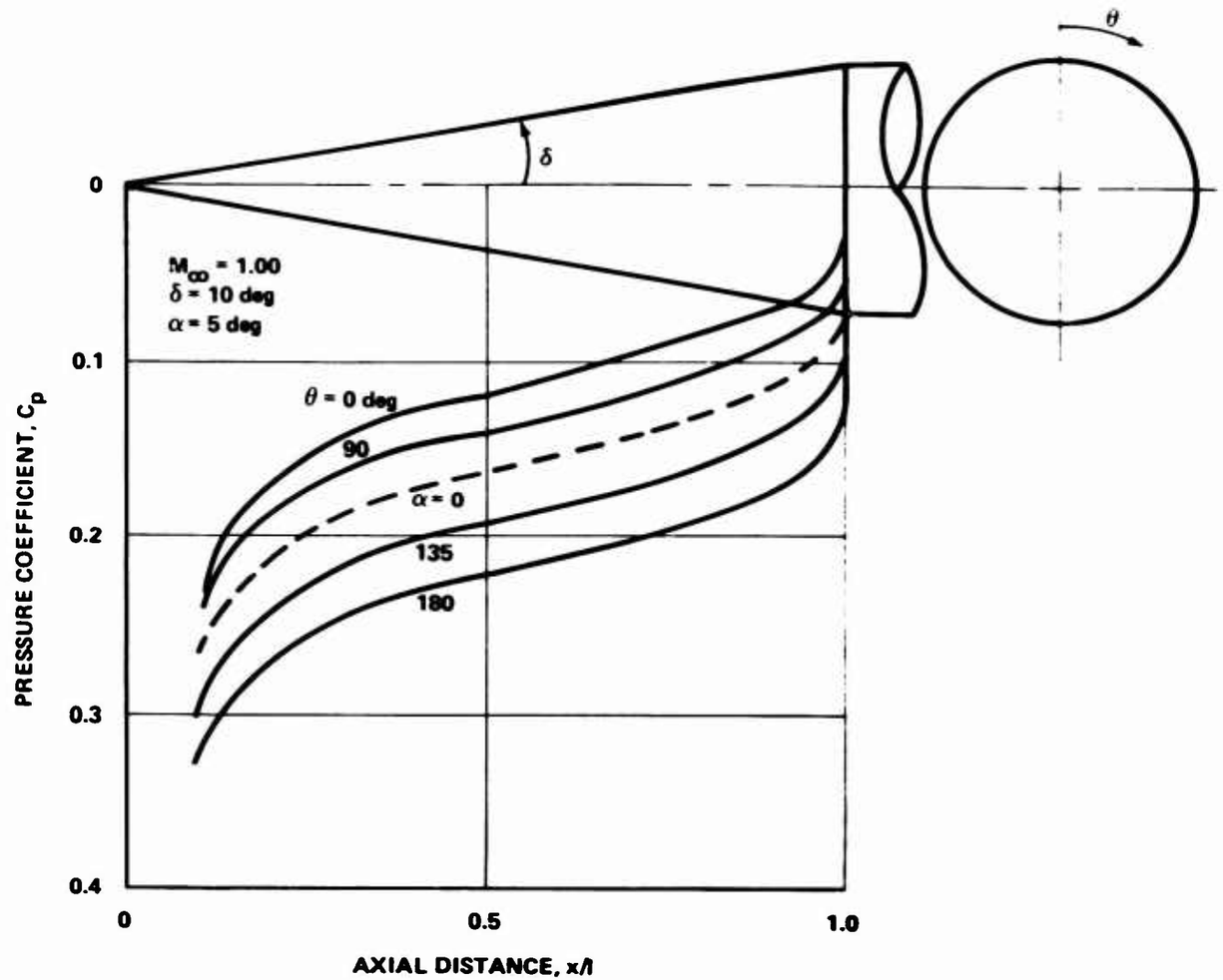

Figure 13. Calculated Flow over Cone at 5-Degree Incidence and M_∞ = 1.0

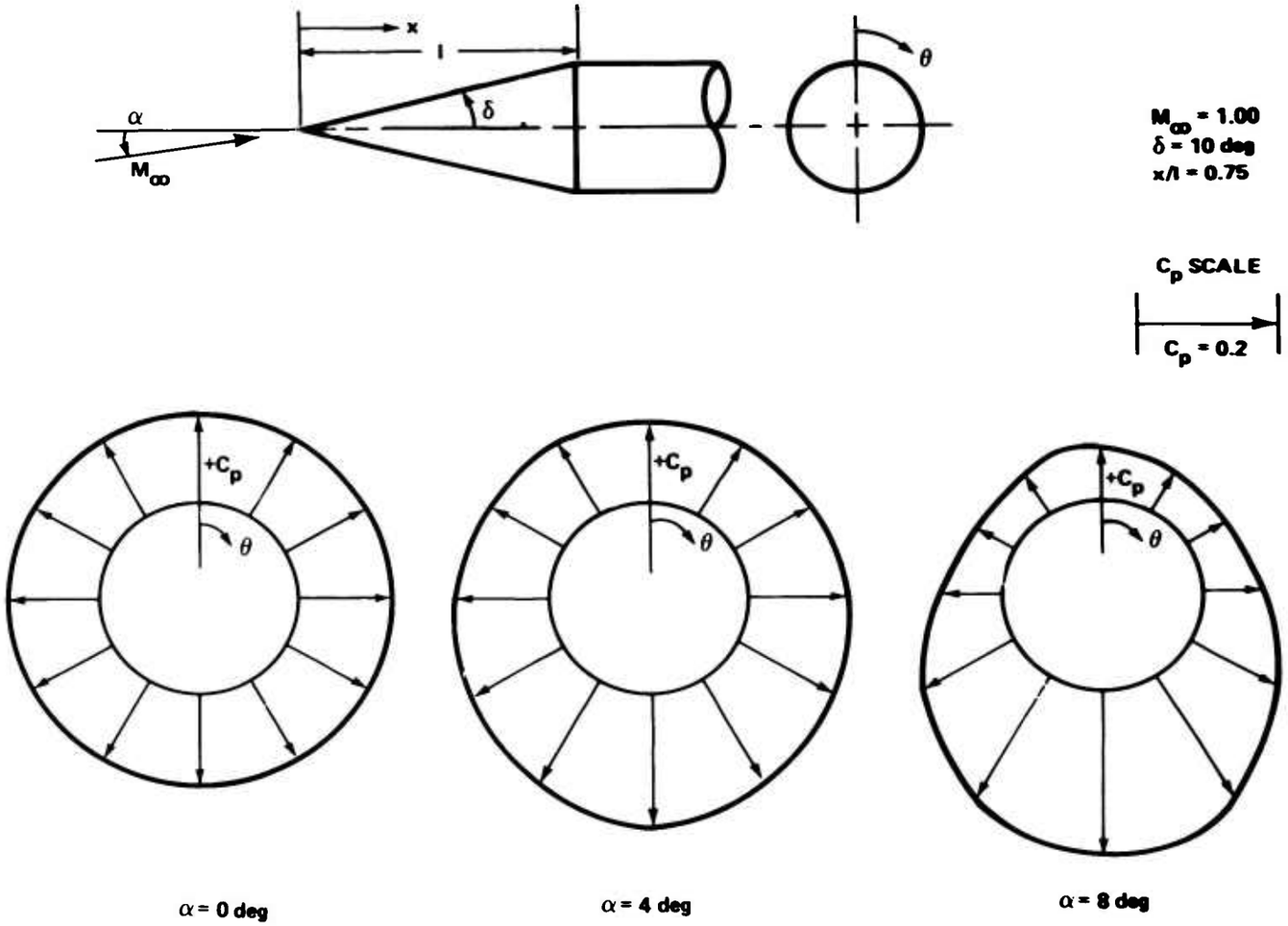

Figure 14. Surface Pressure Distribution on 10-Degree Cone at M_∞ = 1.0 (at x/ℓ = 0.75 Station)

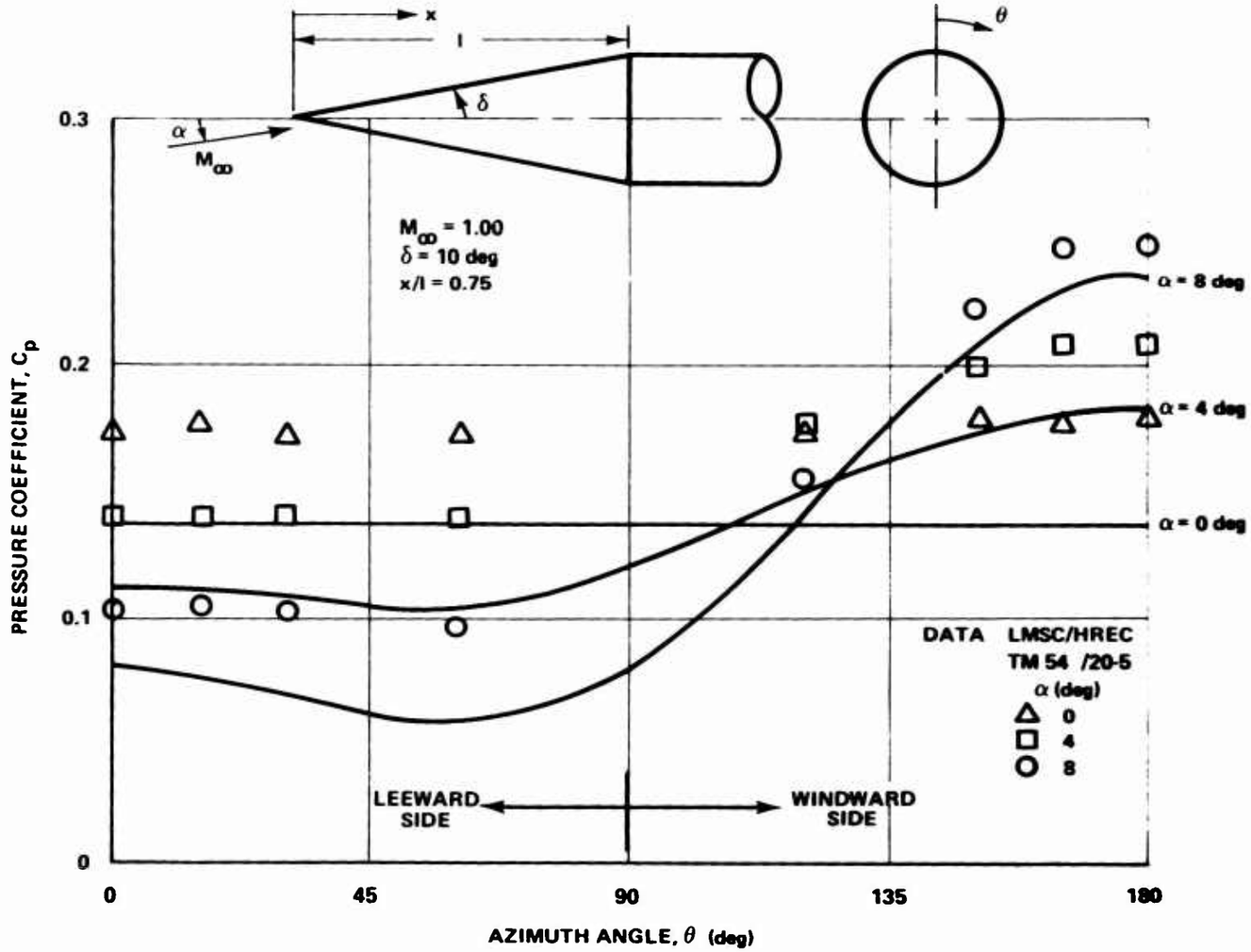

Figure 15. Comparison of Theory with Data for a Cone at Various Angles of Attack

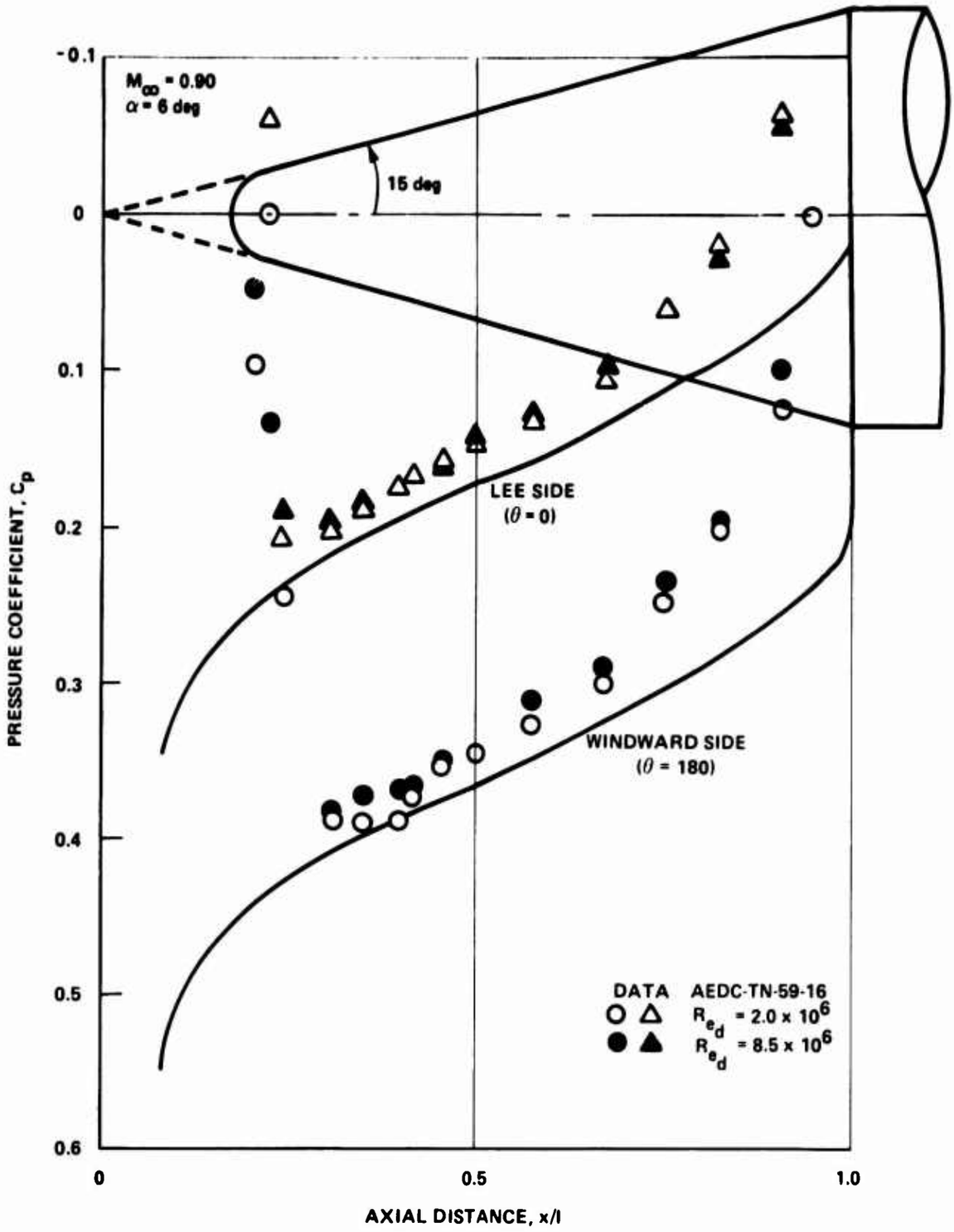

Figure 16. Flow over a Blunted 15-Degree Cone at M_∞ = 0.9

perturbation velocity along the cylindrical portion of the body calculated from the shoulder downstream can be expressed as [3]:

$$u_x = \frac{1}{5} \frac{x - c}{\sqrt{(1+\gamma) M_\infty^{2/3}}} \left[\frac{1}{25} \frac{(x - c)^2}{(1+\gamma) M_\infty^{2/3}} - \frac{1-M_\infty^2}{(1+\gamma) M_\infty^2} \right]^{1/2}$$

and C is given by

$$C^2 = 25\,(1+\gamma) M_\infty^{2/3} \left[\frac{1}{2} \frac{1-M_\infty^2}{(1+\gamma)\, M_\infty^2} + \left\{ \frac{5}{4} \left(\frac{1-M_\infty^2}{(1+\gamma)\, M_\infty^2} \right)^2 + \frac{2}{M_\infty^{2/3}} \frac{1-M_\infty^2}{(1+\gamma) M_\infty^2} \left(\frac{3\delta}{2\sqrt{1+\gamma}} \right)^{2/3} + \left(\frac{3\delta}{2\sqrt{1+\gamma}\, M_\infty} \right)^{4/3} \right\}^{1/2} \right]$$

where δ is the semiapex angle of the cone. The pressure coefficient along the cylinder reads

$$C_p \simeq -\frac{2}{5} \frac{(x - c)}{\sqrt{(1+\gamma)\, M_\infty^{2/3}}} \left[\frac{1}{25} \frac{(x - c)^2}{(1+\gamma) M_\infty^{2/3}} - \frac{1-M_\infty^2}{(1+\gamma) M_\infty^2} \right]^{1/2} .$$

Some typical calculated results compared with experiments are given in Figures 17 through 19 for subsonic, sonic, and supersonic freestream Mach numbers, respectively. The shock condition and the possible boundary-layer separation for subsonic freestream Mach number cases will be discussed in more detail in a report to be published on cone-cylinders in transonic flow*.

*Wu and Aoyama, loc. cit.

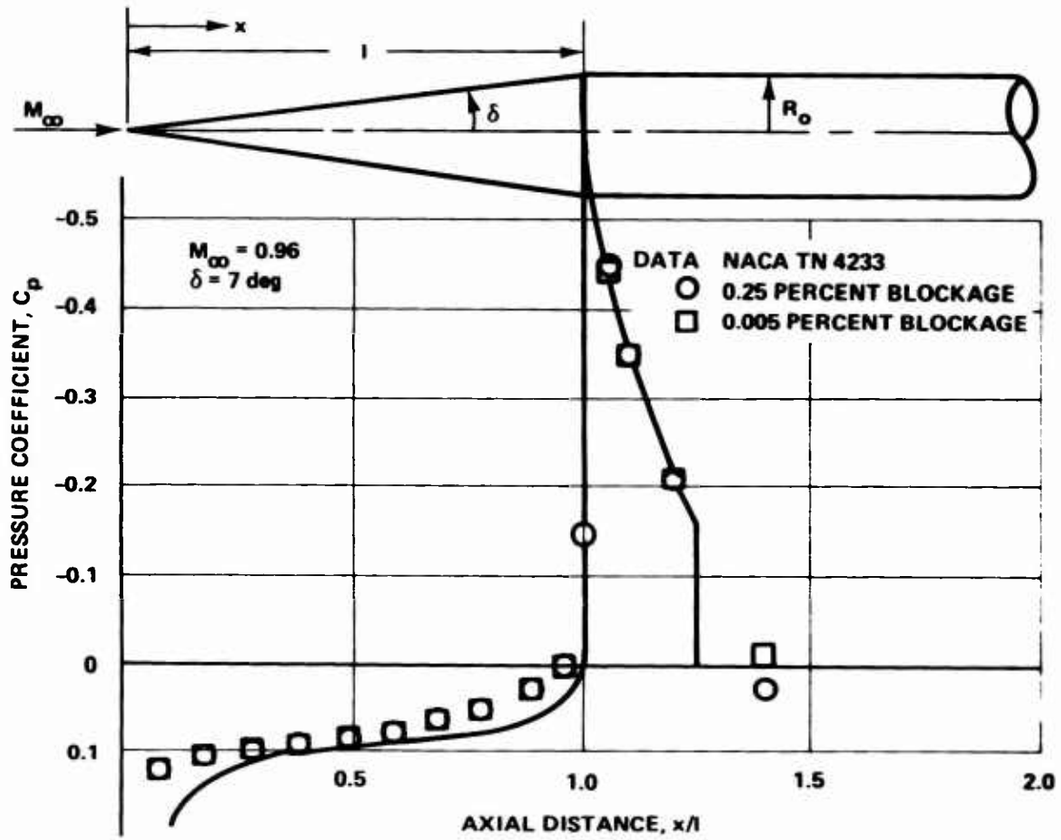

Figure 17. Calculated Flow for Cone Cylindrical Body at M_∞ = 0.96

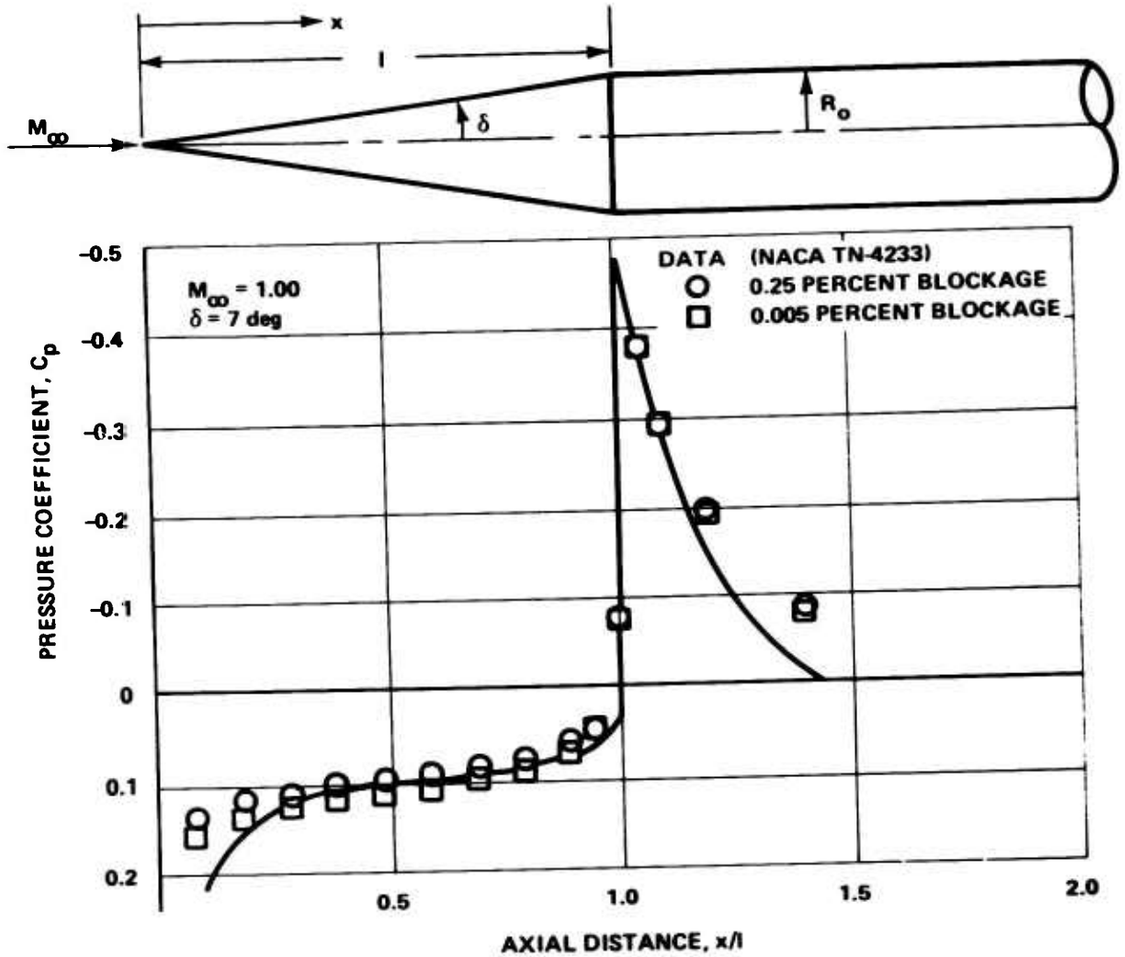

Figure 18. Calculated Flow for Cone Cylindrical Body at M_∞ = 1.00

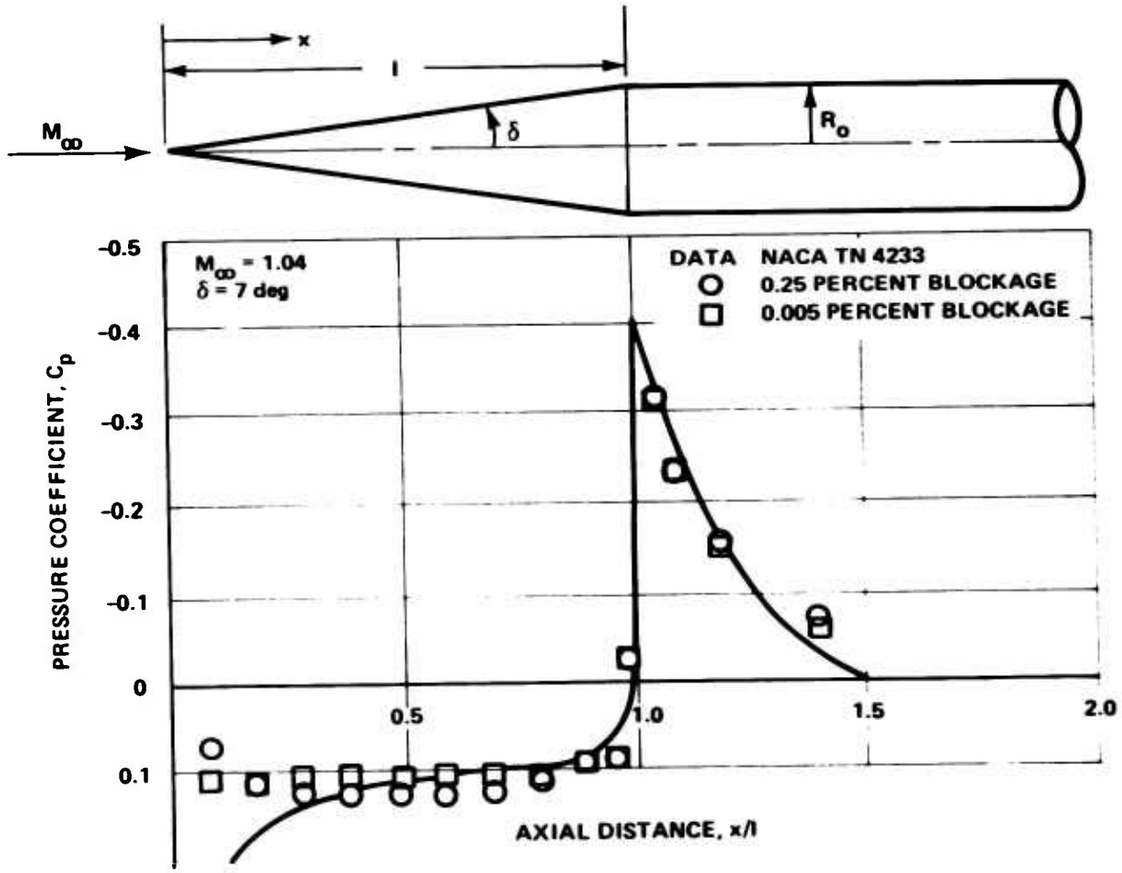

Figure 19. Calculated Flow for Cone Cylindrical Body at M_∞ = 1.04

Section III. CONCERNING VISCOUS EFFECTS

This part of the report discusses two main topics. Paragraph 1 deals with the distortion of the potential flow field due to the development of the boundary-layer on the body surface, while Paragraph 2 concerns the interaction of a jet exhaust plume with the body flow field.

The work described is the first stage in the determination of the entire, viscous, flow over a missile configuration at transonic speeds. It will be shown that such calculations can be performed adequately; with the exception of certain vital components. Areas where little success can be claimed, relate to the turbulent boundary-layer close to separation in a subsonic flow, and to a turbulent boundary-layer developing on a body containing discontinuities in slope. Work is in progress to redress these deficiencies.

1. Studies on Viscous/Inviscid Interactions

Writing the Navier Stokes equations (under the assumption of constant coefficient of viscosity)

$$\frac{D\vec{q}}{Dt} + \frac{1}{\rho}\,\text{grad}\,P = \nu\left[\text{curl curl}\,\vec{q} + \frac{4}{3}\,\text{grad}\,\Delta\right]$$

$$\frac{\partial\rho}{\partial t} + \text{div}\,(\rho\vec{q}) = 0 \qquad (44)$$

where for the general vector $\vec{A}$

$$\frac{D\vec{A}}{Dt} = \frac{\partial\vec{A}}{\partial t} + \frac{1}{2}\,\text{grad}\,A^2 - \vec{A} \times \text{curl}\,\vec{A}$$

and Δ is the dilatation div $\vec{q}$; we consider only steady flow, wherein all temporal derivatives are zero.

Then, writing

$$\vec{q} \simeq \vec{q}_o + \epsilon_1(\lambda)\,\vec{q}_1 + \ldots$$

$$P \sim P_o + \epsilon_1(\lambda)\,P_1 + \ldots$$

$$\rho \sim \rho_o + \epsilon_1(\lambda)\,\rho_1 + \ldots \qquad (45)$$

where $\lambda = 1/Re$ with Re the Reynolds number, and substitution into Equation (44) gives in the limit $\lambda \to 0$

$$\frac{D\vec{q}_o}{Dt} + \frac{1}{\rho_o} \text{ grad } P_o = 0$$

$$\text{div}\left(\rho_o \vec{q}_o\right) = 0 \quad . \tag{46}$$

The subscripts o, 1, and 2 indicate the order of the solutions.

These equations are the classical potential flow equations - if curl $\vec{q}_o = 0$, so that $\vec{q}_o = \text{grad } \varphi_o$

when

$$\text{grad}\left[\frac{1}{2} q_o^2 + \int \frac{dP_o}{\rho_o}\right] = 0$$

$$\text{div}\left(\rho_o \text{ grad } \varphi_o\right) = 0 \quad . \tag{46a}$$

These equations have been solved for transonic flow as discussed in Section II and previous publications [1, 2].

Transforming the independent variables

$$x = X; \; y = Y\lambda^{-1/2}$$

where X, Y ~ O(1), and placing,

$$P \sim P_o^{\,i} + \delta_1(\lambda) P_1^{\,i} + \ldots$$

$$\rho \sim \rho_o^{\,i} + \delta_1(\lambda) \rho_1^{\,i} + \ldots \tag{47}$$

with similar expressions for the velocity components, gives in the limit ($\lambda \to 0$)

$$\operatorname{div}\left(\rho_o^{\,i}\,\vec{q}_o^{\,i}\right) = 0$$

$$u_o^{\,i}\,\frac{\partial u_o^{\,i}}{\partial x} + v_o^{\,i}\,\frac{\partial u_o^{\,i}}{\partial y} + \frac{1}{\rho}\,\frac{dP_o^{\,i}}{dx} = \nu\,\frac{\partial^2 u_o^{\,i}}{\partial y^2} \qquad (48)$$

as the first approximation to the inner expansion (i.e., the classical boundary-layer equations). The solution to these equations will be indicated in Paragraph 2 for laminar and turbulent flow.

Equations (46) and (48) represent the classical solutions to the flow over a body. However, these solutions do not introduce any interaction between the boundary-layer development and the external flow. Only through the evaluation of (at least) the second terms in the sequences [Equations (45) and (47)] can this interaction be accounted for.

To some approximation, it is possible to evaluate the interaction by utilizing the equivalent body concept. Here the boundary-layer displacement surface is added to the geometric body, thus generating an "equivalent body". The potential flow is then determined for this equivalent body and an iteration is established between the body shape and the boundary-layer development.

It should be noted that for steady flow,

$$\frac{1}{2}\,\mathrm{grad}\,q^2 - \vec{q}\times\vec{w} = -\frac{1}{\rho}\,\mathrm{grad}\,P + \nu\left[\mathrm{curl}\,\mathrm{curl}\,\vec{q} + \frac{4}{3}\,\mathrm{grad}\,\Delta\right]$$

so that only if $\nu = 0$ and the vorticity vanishes ($\vec{w} = 0$) is the pressure gradient aligned with the velocity gradient. The assumption of zero vorticity implies an irrotational approaching flow and that any shock waves in the flow are sufficiently weak for their entropy gradients to be ignored. In viscous flow this is not so and the additional terms, ν curl $\vec{w}$, etc must be included. In the equivalent body technique, these terms are forced to be zero outside the displacement surface and the streamlines in the boundary layer do not "match" those of the external flow. The potential flow past an equivalent body does not model the real flow [13]. However, unless the flow is near to separation, the correction is small ($d\delta^*/dx$ small) and the equivalent body technique gives a good result.

Figure 20 presents a typical calculated boundary-layer development for a four calibre tangent ogive body in transonic flow ($M_\infty = 0.975$).

This result is taken from reference [13]. The correction introduced into the calculated surface pressure distribution is presented in Figure 21.

We readily conclude from this result (i.e., Figure 21), that provided the boundary layer is thin, we can ignore the interaction between the boundary layer growth and the external potential flow. This result may seem surprising in a transonic flow where the nonlinearity generally produces rapid changes in the flow with small changes in boundary conditions. More discussions can be found in reference [13].

2. Comments on Plume Induced Separation

The potential flow theories discussed in Section II cannot describe the interaction between an exhaust jet plume and the body flow field because the details of the interaction are intimately controlled by viscous forces in the flow. In this section, some techniques for describing the viscous effects are discussed.

Five major components of the interaction may be isolated. Each will be considered, in term, in the following paragraphs. It should be emphasized that the applicability of the interaction studies presented are restricted to supersonic conditions.

a. The Approaching Boundary Layer

As a necessary initial condition for the shear-layer calculation, the boundary-layer development on the body must be known. It is in this way that changes in the Reynolds number (and boundary-layer transition) influence the interaction between the plume and the body flow field. Once the flow is essentially turbulent, however, further increases in Reynolds number will be of little significance.

The potential flow theory provides the basic pressure distribution from which to calculate the boundary-layer development. Since the current theoretical treatment is only applicable if the flow is supersonic, it is adequate to assume that the presence of the plume does not influence the body pressure field ahead of the interaction. In addition, it was shown [13] that the distortion of the flow field resulting from the boundary-layer development is also negligible for the present purpose. Hence, the boundary-layer development may be estimated directly from the pressure field provided by the theory of reference [2].

Applying the Mangler-Stepanov transformation [14, 15] and the Stewartson-Illingworth transformation [16, 17] to the laminar boundary-layer theory of Thwaites [18] yields the following result for the momentum thickness:

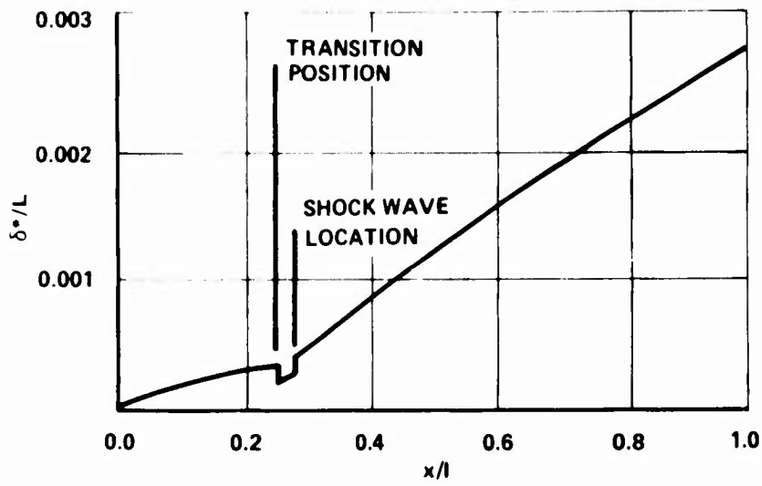

Figure 20. Calculated Boundary Layer for $M_\infty = 0.975$ and Re = $1.2 \cdot 10^6$/ft

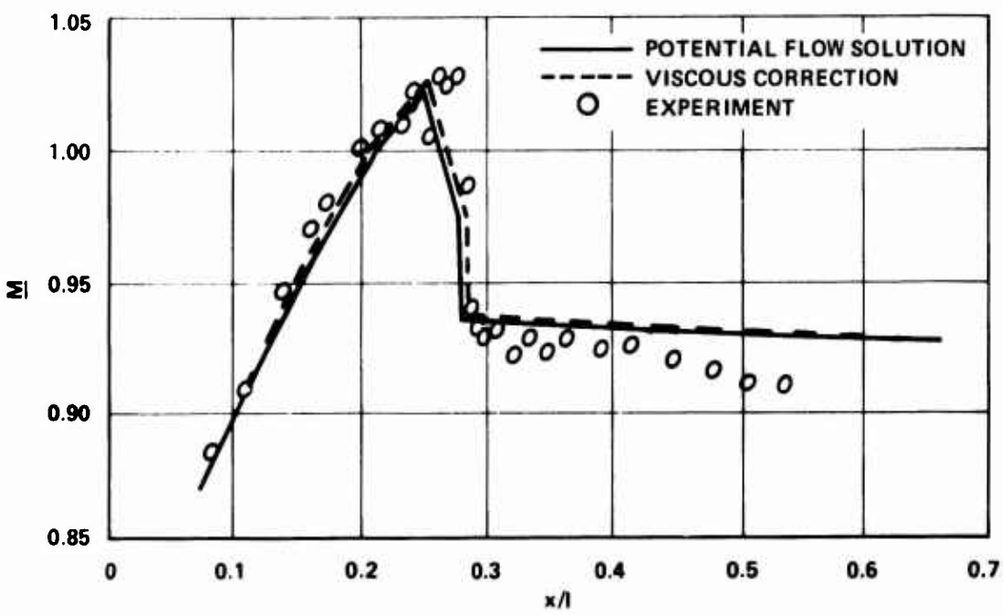

Figure 21. Calculated Correction to Surface Pressure Distribution

$$\left(\frac{\nu}{L}\right)^2 = \frac{0 \cdot 45}{Re(R/L)^2} \left(\frac{U}{U_\infty}\right)^{-6} \left(\frac{T_\infty}{T_o}\right)^{\frac{2-\gamma}{\gamma-1}} \left(\frac{T_e}{T_\infty}\right)^{\frac{2\gamma-4}{\gamma-1}} \int_o^{x/L} \left(\frac{U}{U_\infty}\right)^5 \left(\frac{T_e}{T_\infty}\right)^{\frac{2-\gamma}{\gamma-1}} \left(\frac{R}{L}\right)^2 d(x/L).$$

The nondimensional pressure gradient, (Γ), is

$$\Gamma = \frac{\nu^2}{\nu} \left(\frac{T_\infty}{T_e}\right)^{\frac{\gamma-2}{\gamma-1}} \frac{dU}{dx}$$

then the form factor and skin friction coefficient are related to the function Γ by the empirical relations given by Thwaites. Some details are also given in reference [19].

Transition of the laminar boundary layer was considered to occur either at some prescribed location (e.g., as dictated by experimental evidence) or when the Reynolds number,

$$\frac{U_\infty \delta^*}{\nu} = 900,$$

is reached locally in the flow. This latter criterion was taken from the experimental data presented in reference [20]. If boundary-layer separation was predicted before the satisfaction of the above Reynolds number criterion, then the separation point was used as the point of transition. Note, that separation is taken to be when $\Gamma = -0.09$.

To complete the boundary-layer calculation, the turbulent boundary-layer theory of Nash [21] was used. This integral theory, based upon the momentum integral equation,

$$\frac{1}{R} \frac{d}{dx} \left(\rho_e U_e^2 R\theta\right) = \tau_w - \rho_e U_e \frac{dU_e}{dx} \delta^*$$

is applicable to compressible, axisymmetric flow. The shear stress integral is taken to satisfy a differential equation which (at least heuristically) is representative of turbulence phenomena (and is somewhat reminiscent of the equation of Burgers [22]).

Finally, if the boundary layer encounters a discontinuity in pressure distribution (weak shock-wave or expansion fan) then it is

assumed that the boundary-layer momentum thickness suffers a discontinuity given by

$$\theta_2/\theta_1 = \rho_1 V_{e_1} M_{e_1}^2 \Big/ \rho_2 V_{e_2} M_{e_2}^2 \quad .$$

The applicability of this equation to a sudden expansion (e.g., supersonic flow over a boat tail configuration) is open to speculation. Thus, it is shown in Figure 22 that the boundary-layer development on such a boat tail is extremely sensitive to changes in the initial conditions after the expansion. The result quoted by White [23], being of the same form as the above equation, is not sufficiently different to give more satisfactory results. In addition, according to the data of Rubin [24], there can be a significant acceleration of the flow ahead of the boat tail. The assumption of a discontinuous velocity change at the boat tail is not adequate and a more detailed theory for this region is required.

b. Turbulent Boundary-Layer Separation

In the case of a rapid separation of a turbulent boundary layer in supersonic flow, the approximate theory of Mager [25] may be used. Although designed for two-dimensional flow, the result shown in Figure 23 indicates that the pressure rise to separation in axially symmetric flow may also be estimated by this method. The experimental data shown in Figure 23 is taken from Kuehn [26].

The data from reference [26] also shows that above a Reynolds number of $R_\delta \sim 10^5$, the pressure rise to separation is little influenced by increase in Reynolds number. Indeed, the data in reference [27] suggests a variation like $Re^{-1/40}$ (which is considerably smaller than the $Re^{-1/8}$ variation predicted by Ray [28]). For the present study, we neglect the influence of Reynolds number on the pressure rise to separation. Reynolds number then only enters the calculation as it influences the boundary-layer momentum thickness at the start of the interaction. It is considered that this neglect of Reynolds number on the pressure rise to separation is of higher order than the accuracy of the basic theory (Figure 23) for separation prediction.

It is also shown in reference [26] that the sensitivity of a boundary layer to separation is a function of the velocity profile. The further removed the profile is from its equilibrium value, the more easily will the boundary layer separate. This point will be of significance in the later discussion on the flow past a body with a boat tail.

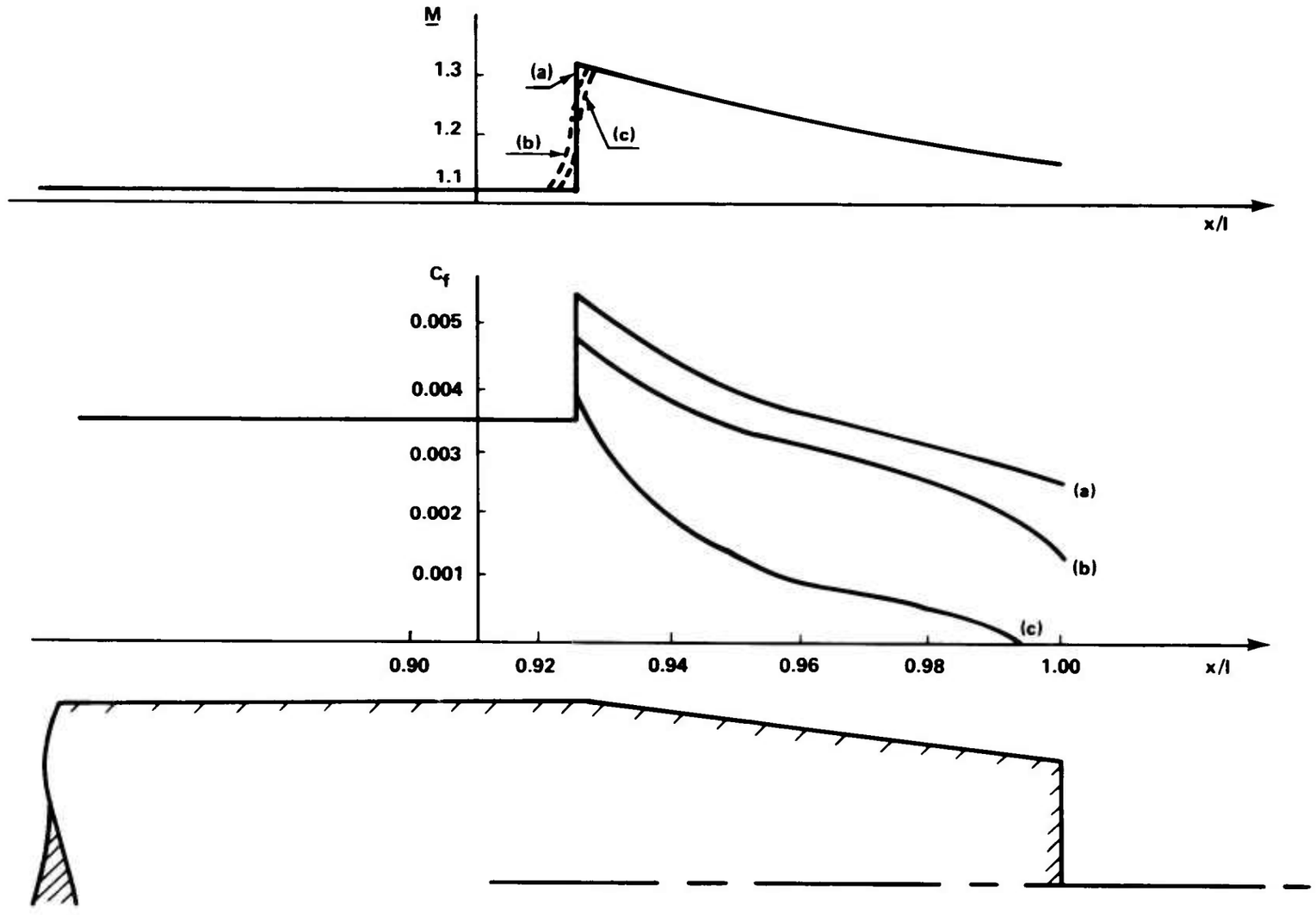

Figure 22. Sensitivity of Boat Tail Boundary Layer to Initial Conditions

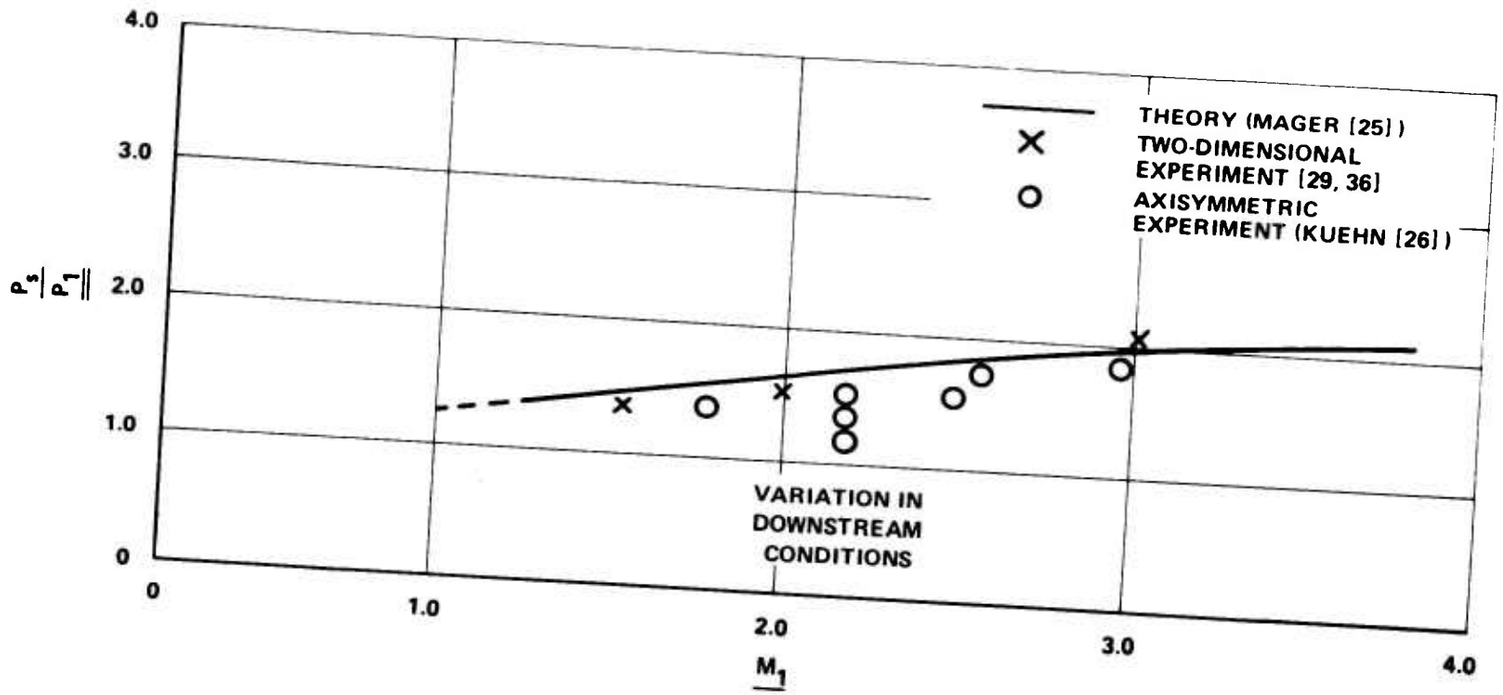

Figure 23. Comparison of Separation Pressures in Two-Dimensional Axisymmetric Flow (Turbulent Boundary Layers)

The pressure rise to separation also depends on the downstream conditions (Figure 23). Although this result is contrary to the usually accepted situation in supersonic separation (as embodied in the results of reference [29]), it is physically reasonable to expect some small dependence on downstream conditions resulting from the reversed flow in the separation region. This point is of significance in the plume induced separation problem where the downstream conditions (plume shape and shear layer confluence) depend upon the jet pressure ratio. It is hoped that future developments can go towards evaluating the magnitude of this "upstream influence."

The equations of Paragraph 1 determine the boundary-layer momentum thickness at the start of the interaction. Following the suggestion of McDonald [30], this momentum thickness may be related to that at the start of the shear layer by the relation:

$$\theta = \theta_o \left[\frac{1+\frac{\gamma-1}{2} M_2^2}{1+\frac{\gamma-1}{2} M_1^2} \right]^3 \left[1 - 0.605\, Cp + 11.725\, Cp^2 \right]$$

where

$$Cp = 1 - M_2^2 / M_1^2$$

and M_1 is the Mach number ahead of the shock, M_2 the Mach number behind the shock, and θ_o the boundary-layer momentum thickness at the start of the interaction.

c. Free Shear Layer

It is assumed (following Kirk [31]) that the free shear layer leaving the body surface at the separation point can be replaced by some equivalent asymptotic shear layer; the correct asymptotic layer being selected by matching momentum thicknesses between the shear layer and the separated boundary layer at the separation point. Clearly, as the free shear layer is reduced in length (compared to its width) the utility of the equivalent shear layer concept is reduced. In cases where the flow is not much different from that in a bubble, the concept is entirely inappropriate.

Since we have included the effect of the boundary layer on the shear layer development, the results are more sophisticated than those obtained by Dixon et al. [32] or Schulz [33] and go, at least some way, towards including Reynolds number effects.

The flow equations in the asymptotic shear layer were described in reference [1] and need not be repeated here.

The unknown constant (the boundary-layer momentum thickness at the start of the shear layer) is determined from the boundary-layer calculation outlined in Paragraph a and the relation across the interaction given in Paragraph b.

d. Jet Plume

Initial calculations have been performed using the plume geometry developed empirically by Herron [34]. Further details were given in reference [1]. At the same time, a more complete calculation using the method of characteristics program developed by Prozan [35] is being undertaken.

e. Conditions at Confluence

We follow Korst and assume that the final static pressure after the recompression is equal to the stagnation pressure on the dividing streamline before the confluence. Figure 24 shows this diagramatically.

If it is assumed that the recompression is isentropic, then

$$P_f = P_i \left(1 + \frac{\gamma-1}{2} M_s^2\right)^{\gamma/\gamma-1}$$

where P_f and P_i are the static pressures before and after the recompression, and M_s is the Mach number on the dividing streamline.

For the isoenergic flow, we have:

$$M_s^2 = \frac{2}{\gamma-1} C_\infty^2 \quad (u/Ue)^2 \Big/ \left[1 - C_\infty^2 \ (u/Ue)^2\right]$$

with

$$C_\infty^2 \equiv \frac{\gamma-1}{2} M_\infty^2 \Big/ \left[1 + \frac{\gamma-1}{2} M_\infty^2\right]$$

and u/Ue is the velocity distribution in the approaching shear-layer.

Figure 24. The Confluence Region

The solution of the confluence region is closed by means of the relations between pressure change and turning angle in linearized supersonic flow. The solution is valid only when the flow downstream of the surface separation is supersonic because this supersonic turning angle is assumed.

f. Calculated Results

A typical missile configuration (4-calibre tangent ogive body) was used to obtain data on plume effects (Figure 25).

Initial calculations were performed at a free stream Mach number 2 on the body shown in Figure 25 without the boat tail. The extent of separation as a function of jet pressure ratio is shown in Figure 26.

The calculations were repeated at a free stream Mach number 1.1. Again the body was taken without the boat tail. For low jet pressure ratio ($P_J \sim 10\ P_\infty$), it is seen in Figure 27 that no flow separation is present. At significantly higher pressure ratios, separation is produced.

Figure 28 presents two important points. First, it is shown that variation in the boundary-layer transition point has very little influence on the location of the plume induced separation point. Only when the transition occurs in the immediate vicinity of the separation point will the flow exhibit a significant variation with the actual location of transition. Secondly, Figure 28 shows that the influence of the plume has provoked separation of the boundary layer ahead of the point of separation predicted by the boundary layer calculation in the absence of the plume.

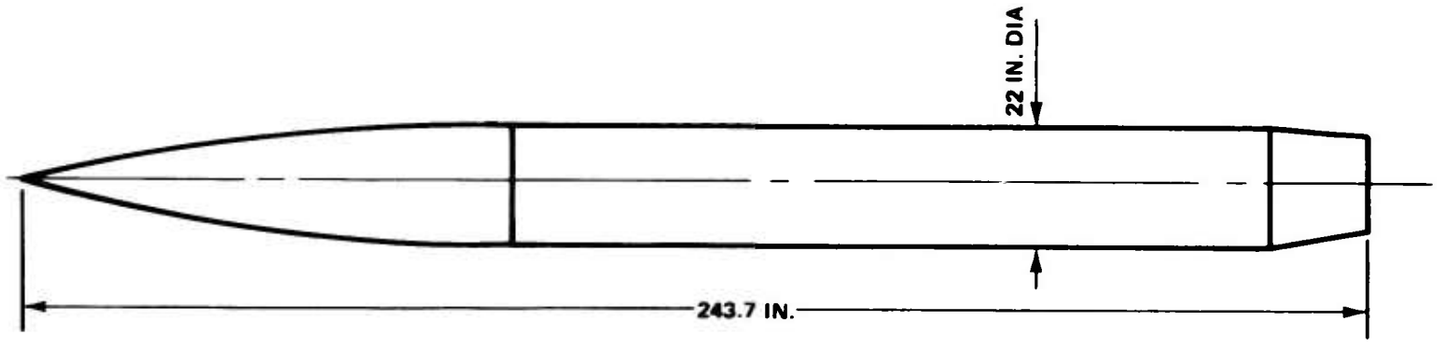

Figure 25. Four-Calibre Tangent Ogive Body Used in Plume Study Calculations

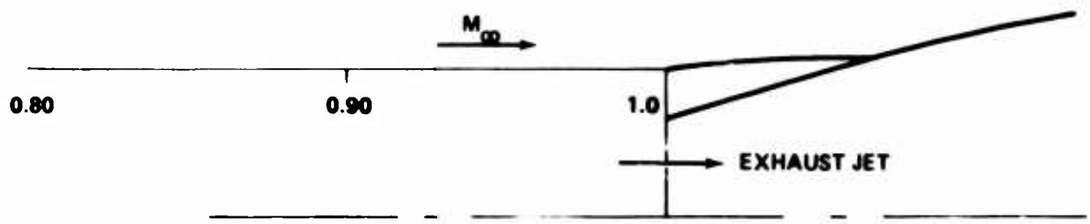

a) FLOW GEOMETRY FOR $M_\infty = 2.0$; $P_J = 2.75$

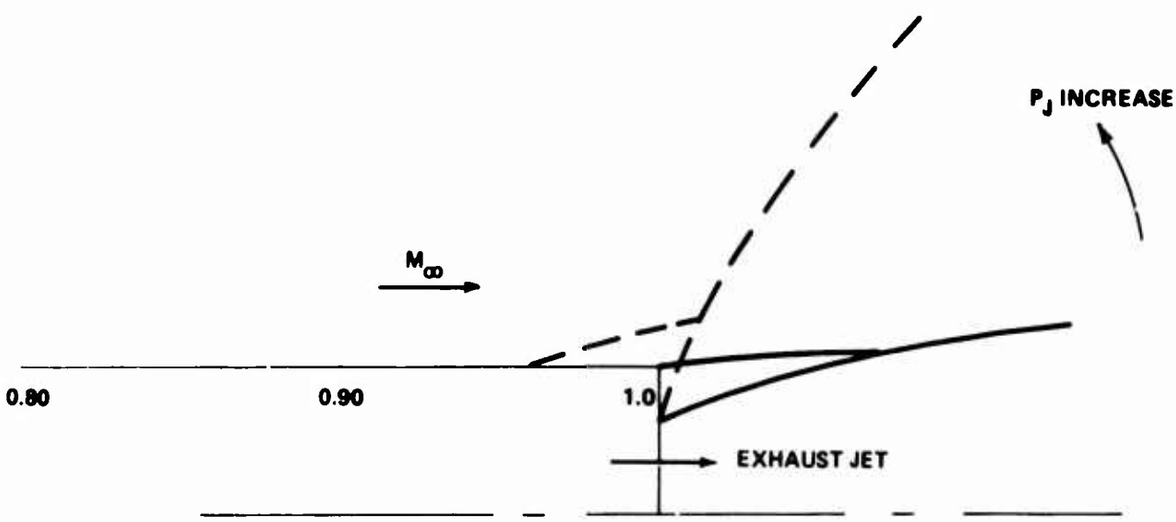

b) EFFECT OF INCREASING JET PRESSURE RATIO $M_\infty = 2.0$

Figure 26. Some Results at $M_\infty = 2.0$

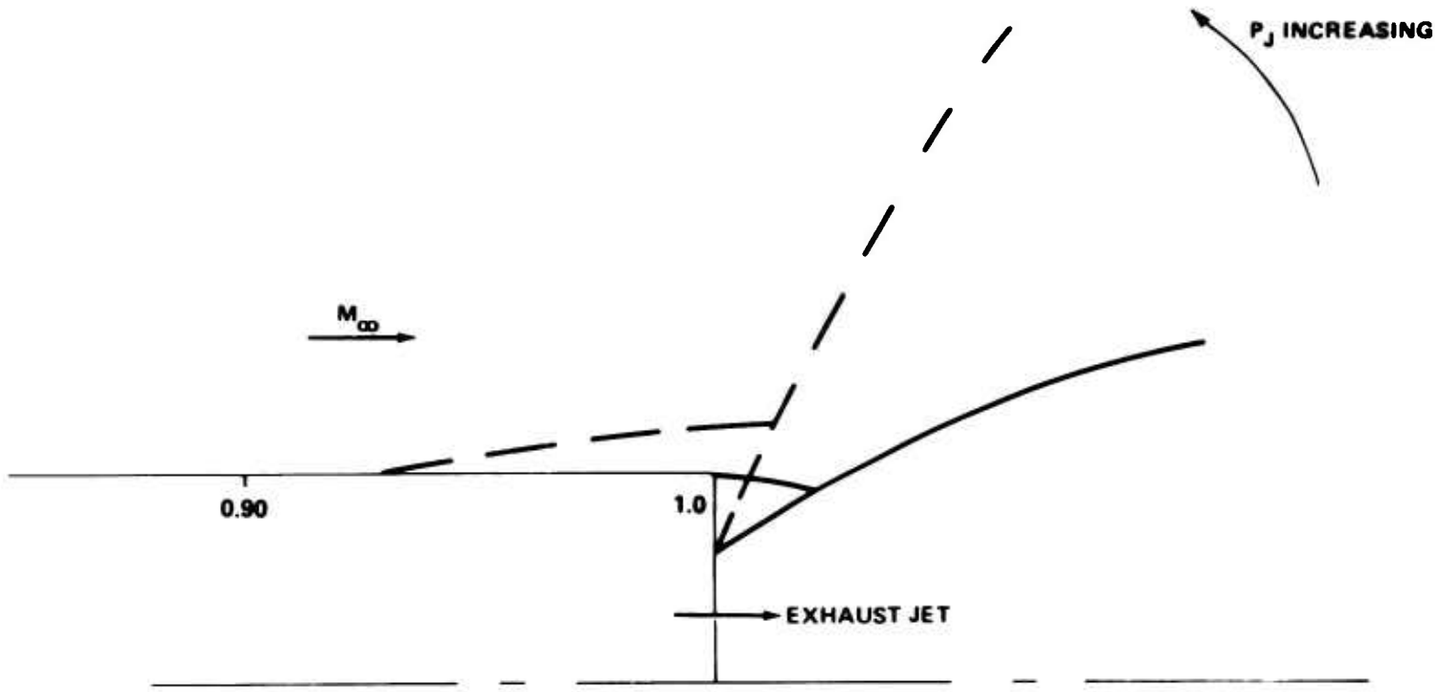

Figure 27. Increase of Flow Separation with Jet Pressure Ratio at $M_\infty = 1.1$

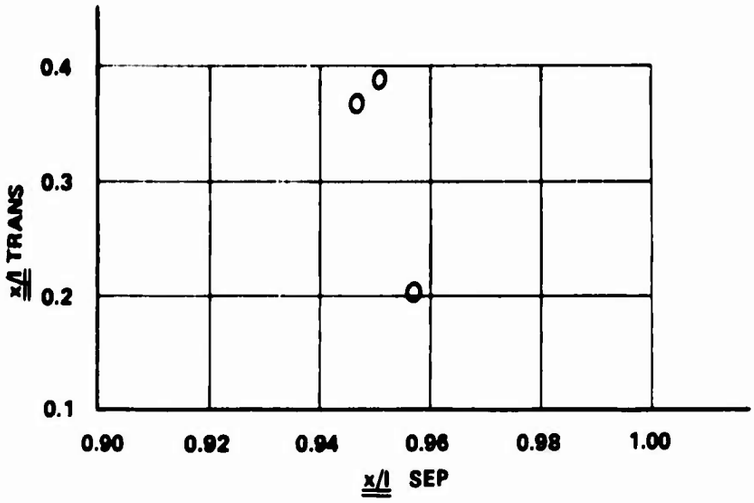

a) EFFECT OF BOUNDARY-LAYER TRANSITION POSITION ON LOCATION OF PLUME-INDUCED SEPARATION.

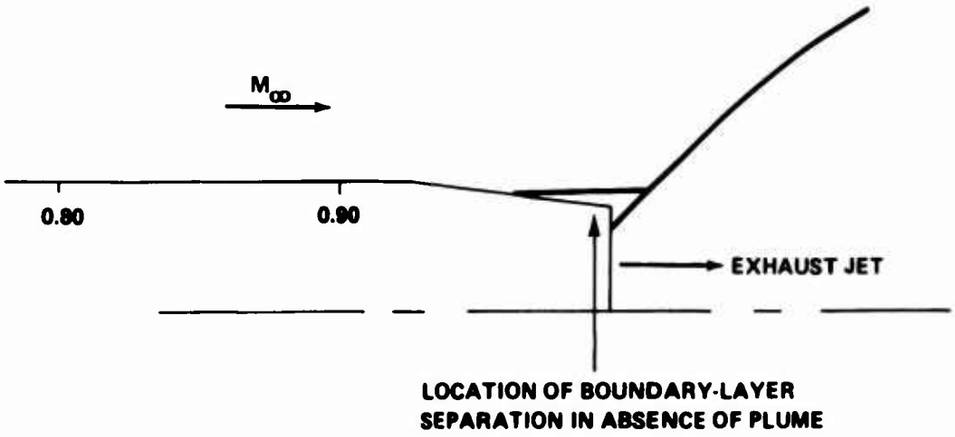

b) GEOMETRY OF PLUME-INDUCED SEPARATION $P_J \sim O(1000)$

Figure 28. Interaction of Plume with Fore-Body Flow at $M_\infty = 1.1$

Section IV. CONCLUSIONS AND RECOMMENDATIONS

A fairly complete understanding of the inviscid transonic flow over various bodies of revolution was obtained during this study. Engineering methods for the computation of the flow over an ogive-cylindrical body with small angle of attack, the conical nose with and without angle of attack and the cone-cylindrical body at zero angle of attack were developed. The analytical results check very well with the available experiments. This increases our level of confidence in the analysis discussed herein.

Many improvements are still needed to obtain more general solutions. For instance, application of the existing theory to an arbitrary shaped smooth body (including the acceleration and deceleration portions) is very desirable. The improved solution around the apex point and the shoulder for a cone-cylindrical configuration should also be studied. To include the angle of attack, or the effect due to the cross-flow, on the local two-dimensional method is another subject needing careful study.

It was found that the viscous effects on an ogive-cylindrical body are not too significant. However, estimation of the viscous effects applicable to the boat tail portion needs specific attention. Our preliminary viscous analysis indicates that the shoulder of a boat tail is very crucial to the boundary layer separation caused by the exhaust jet plume.

The calculation of an entirely subsonic or a mixed supersonic/subsonic seperation will form the subject of further study.

REFERENCES

1. Wu, J. M , Aoyama, K., and Moulden, T. H.; Study of Flow Around Axisymmetric Bodies with and Without Plume Induced Separation at Transonic Speeds - Summary Report; U S. Army Missile Command, Redstone Arsenal, Alabama, Technical Report No. RD-TR-70-3; March 1970 .

2. Wu, J. M. and Aoyama, K., Transonic Flow-Field Calculation Around Ogive Cylinders by Nonlinear – Linear Stretching Method, U. S. Army Missile Command, Redstone Arsenal, Alabama, Technical Report No. RD-TR-70-12, April 1970. Also AIAA 8th Aerospace Sciences Meeting, AIAA Paper, January 1970, pp. 70-189.

3. Wu, J. M. and Aoyama, K., Pressure Distributions for Axisymmetric Bodies with Discontinuous Curvature in Transonic Flow, U. S. Army Missile Command, Redstone Arsenal, Alabama, Technical Report No. RD-TR-70-25, November 1970.

4. Hosokawa, I., "A Refinement of the Linearized Transonic Flows Around Thin Bodies", J. Phys. Soc., Japan, Vol. 15, 1960, pp. 149-157.

5. Hosokawa, I., "A Simplified Analysis for Transonic Flows Around Thin Bodies", Symposium Transonicum, Editor, K. Oswatitsch, Springer-Verlag, Berlin, 1964, pp. 184-199.

6. Oswatitsch, K. and Keune, F., "The Flow Around Bodies of Revolution at Mach Number One", Proceedings of the Conference on High-Speed Aeronautics, Polytechnique Institute of Brooklyn, January 1955.

7. Liepmann, H. W. and Roshko, A., Elements of Gas Dynamics, John Wiley and Son, Inc., New York, 1957.

8. Cole, J. D. and Royce, W. W., "An Approximate Theory for the Pressure Distribution and Wave Drag of Bodies of Revolution at Mach Number One", Proc. 6th Midwestern Co ıference on Fluid Mechanics, 1959, pp. 254-276.

9. Sprieter, J. R. and Alksne, Y., Slender Body Theory Based on Approximate Solution of the ansonic Flow Equation, NASA Technical Report, R-2, 1959.

10. Yashihara, H., On the F ver a Cone-Cylinder Body at Mach Number One, WADC Technic. Report 52-295, 1952.

11. Leiter, E. and Oswatitsch, K., "Ermittlung Stationärer Schallnaher Strömung in Absteigenrerfahren aus dem Instationaren, ZAMM, Vol. 48, 1968, S. 187-191.

PRECEDING PAGE BLANK

12. Page, W. H., Experimental Study of the Equivalence of Transonic Flow About Slender Cone-Cylinders of Circular and Elliptic Cross Section, NACA Technical Note 4233, 1958.

13. Moulden, T. H., Spring, D. J., Saisi, R. O., Aoyama, K., and Wu, J. M.; Bodies of Revolution at Transonic Speeds: The Estimation of Reynolds Number Effects; Paper to AGARD Specialists Meeting on "Facilities and Techniques for Aerodynamic Testing at Transonic Speeds and High Reynolds Numbers"; Göttingen; April 26-28, 1971.

14. Mangler, W., "Zusammenbang Zwischen Ebenen und Rotation Asymmetrischen Grenzschichter in Kompressiblen Medien", ZAMM, Vol 28, 1948, p. 97.

15. Stepanov, E. I., "On the Integration of the Laminar Boundary-Layer Equations for a Motion with Axial Symmetry", PMM, Vol. 11, 1947, p. 203.

16. Stewartson, K., "Correlated Incompressible and Compressible Boundary-Layers", Proc. Roy. Soc., Vol. 200, 1949, p. 84.

17. Illingworth, C. R., "Steady Flows in the Laminar Boundary-Layer", Proc. Roy. Soc., Vol A199, 1949, p. 533.

18. Thwaites, B., "Approximate Calculation of the Laminar Boundary-Layer", Aero. Quart., Vol. 1, 1949, p. 245.

19. Moulden, T. H. and Wu, J. M., An Outline of Methods Applicable to Viscous Fluid Flow Problems, U. S. Army Missile Command, Redstone Arsenal, Alabama, Technical Report No. RD-TR-71-4, March 1971.

20. Czarnecki, K. R. and Jackson, M. W., Effects of Nose Angle and Mach Number on Transition on Cones at Supersonic Speeds, NACA Technical Note 4388, 1958.

21. Nash, J. F., A Practical Calculation Method for Compressible Turbulent Boundary-Layers in Two-Dimensional Flows, Lockheed Georgia Research Memorandum ER-9428, 1967.

22. Burgers, J. M., "A Mathematical Model Illustrating the Theory of Turbulence", Advances in Applied Mechanics, Vol. 1, Academic Press, 1948.

23. White, R. A., Turbulent Boundary-Layer Separation from Smooth Convex Surfaces in Supersonic Two-Dimensional Flow, Ph. D. Thesis, Mechanical Engineering Department, University of Illinois, Urbana, Illinois, 1963.

24. Rubin, D. V., A Transonic Investigation of Jet Plume Effects on Base and Afterbody Pressures of Boattail and Flare Bodies of Revolution, U. S. Army Missile Command, Redstone Arsenal, Alabama, Technical Report No. RD-TR-70-10, 1970.

25. Mager, A., "On the Model of the Free Shock-Separated, Turbulent Boundary-Layer", Journal Aeronautical Science, Vol. 23, 1956, p. 181.

26. Kuehn, D. M., Turbulent Boundary-Layer Separation Induced by Flares on Cylinders at Zero Angle of Attack, NASA Technical Report R-117, 1961.

27. Chapman, D. R., Kuehn, D. M., and Larson, H. K.; Investigations of Separated Flows in Supersonic and Subsonic Streams with Emphasis on the Effects of Transition; NACA Report No. 1356, 1958.

28. Ray, A. K., "Estimation of the Critical Pressure Rise for Separation in Two-Dimensional Shock Boundary-Layer Interaction Problems", Z. Flugwiss, Vol. 6, 1962, p. 237.

29. Bogdonoff, S. M. and Keppler, C. E., "Separation of a Supersonic Turbulent Boundary-Layer", Journal Aeronautical Science, Vol. 22, 1955, p. 414.

30. McDonald, H., "A Study of the Turbulent Separated Flow Region Occurring at a Compression Corner in Supersonic Flow", JFM, Vol. 22, 1965, p. 481.

31. Kirk, F. N., An Approximate Theory of Base Pressure in Two-Dimensional Flow at Supersonic Speeds, RAE Technical Note Aero. 2377, 1959.

32. Dixon, R. J., Richardson, J. M., and Page, R. H.; "Turbulent Base Flow on an Axisymmetric Body with a Single Exhaust Jet"; J. Spacecraft; Vol. 7; 1970; p. 848.

33. Schulz, R., Rocket Exhaust Plumes in a Separated Supersonic External Stream, M. S. Thesis, University of Tennessee Space Institute, Tullahoma, Tennessee, 1970.

34. Herron, R. D., "Jet Boundary Simulation Parameters for Underexpanded Jets in a Quiescent Atmosphere", J. Spacecraft, Vol. 5, 1968, p. 1155.

35. Prozan, R. J., Development of a Method of Characteristics Solution for Supersonic Flow of an Ideal, Frozen or Equilibrium Reacting Gas Mixture, LMSC/HREC A 782535, April 1966.

36. Seddon, J., The Flow Produced by Interaction of a Turbulent Boundary-Layer with a Normal Shock Wave of Strength Sufficient to Cause Separation, RAE Technical Memorandum Ae 667, 1960.